Accepted Manuscript

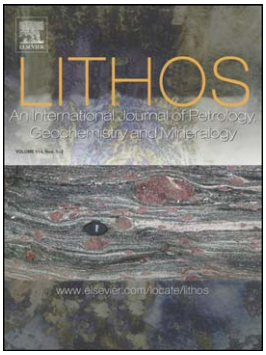

Mixed pyroxenite-peridotite sources for mafic and ultramafic dikes from the Antarctic segment of the Karoo continental flood basalt province

Jussi S. Heinonen, Arto V. Luttinen, Teal R. Riley, Radoslaw M. Michallik

PII: S0024-4937(13)00176-X
DOI: doi: 10.1016/j.lithos.2013.05.015
Reference: LITHOS 2998

To appear in: *LITHOS*

Received date: 28 December 2012
Accepted date: 23 May 2013

Please cite this article as: Heinonen, Jussi S., Luttinen, Arto V., Riley, Teal R., Michallik, Radoslaw M., Mixed pyroxenite-peridotite sources for mafic and ultramafic dikes from the Antarctic segment of the Karoo continental flood basalt province, *LITHOS* (2013), doi: 10.1016/j.lithos.2013.05.015

This is a PDF file of an unedited manuscript that has been accepted for publication. As a service to our customers we are providing this early version of the manuscript. The manuscript will undergo copyediting, typesetting, and review of the resulting proof before it is published in its final form. Please note that during the production process errors may be discovered which could affect the content, and all legal disclaimers that apply to the journal pertain.

ACCEPTED MANUSCRIPT

Mixed pyroxenite-peridotite sources for mafic and ultramafic dikes from the Antarctic segment of the Karoo continental flood basalt province

Jussi S. Heinonen

Finnish Museum of Natural History, P.O. Box 17, University of Helsinki, FI-00014, Helsinki, Finland

Arto V. Luttinen

Finnish Museum of Natural History, P.O. Box 17, University of Helsinki, FI-00014, Helsinki, Finland

Teal R. Riley

British Antarctic Survey, Madingley Road, High Cross, Cambridge, CB3 0ET, United Kingdom

Radoslaw M. Michallik

Department of Geosciences and Geography, P.O. Box 64, University of Helsinki, FI-00014, Helsinki, Finland

CORRESPONDING AUTHOR INFORMATION:

Dr. Jussi S. Heinonen, postdoctoral researcher

Finnish Museum of Natural History

P.O. Box 17 (Arkadiankatu 7)

00014 University of Helsinki

Finland

work phone: +358 40 5765388

email: jussi.s.heinonen@helsinki.fi

ACCEPTED MANUSCRIPT

ACCEPTED MANUSCRIPT

Abstract

Primitive rocks that are related to continental flood basalts are rare, but often reveal crucial information on the ultimate sources of these huge outpourings of mantle-derived magma. Here we present mineral chemical data for mafic and ultramafic dikes from the Antarctic extension of the Jurassic (~180 Ma) Karoo continental flood basalt province that was emplaced during the initial stages of the breakup of the Gondwana supercontinent. We concentrate on two previously recognized high-Ti dike rock suites (Group 3 and Group 4) that exhibit high MgO contents (up to 22 wt. %). Both groups are characterized by Mg-rich olivine phenocrysts (up to Fo_{90}) that are not mantle xenocrysts and indicate derivation from relatively Mg-rich parental magmas. Orthopyroxene is a common phenocryst and groundmass phase indicating emplacement at mid-crustal pressures (2–5 kbar; depth of ~10–20 km). The parental magmas of Group 3 and Group 4 dikes can be associated with pyroxenite sources on the basis of high olivine NiO, high whole-rock Zn/Fe, and low whole-rock CaO. In the case of Group 3 dikes, however, the samples that contain the most Mg-rich olivine also exhibit the mildest pyroxenite fingerprint and indications of an additional olivine-bearing (peridotitic) source component. We propose that the pyroxenite fingerprint of Group 3 and Group 4 dikes reflects relatively low-degree melting of fertile mantle at high pressures beneath the thick and cold Gondwanan lithosphere. Such conditions limited high-degree melting of peridotite sources which may have been predominant in the generation of the Karoo low-Ti basalts within lithospheric thinning zones.

Keywords: Large igneous province; Continental flood basalt; Karoo; Picrite; Pyroxenite; Mantle source

ACCEPTED MANUSCRIPT

1. Introduction

The origins of continental flood basalts (CFBs) have divided scientists for decades, since these manifestations of large-scale mantle melting do not easily fit into accepted plate tectonic theory. A broad range of models have been proposed to explain their petrogenesis and geological characteristics (see Bryan & Ernst 2008; Macdougall 1988; Saunders 2005). Many of the discussions have focused on the relative contribution of the deep mantle, i.e. mantle plumes (e.g., Campbell, 2005; Campbell and Griffiths, 1990; Richards et al., 1989), and lithospheric processes (e.g., Anderson, 1994, 2005; Coltice et al., 2007; Elkins-Tanton, 2005) in their generation. The debate on the origin of CFBs is largely fueled by the absence of detailed information on the parental magmas and the mantle sources involved. This stems from the fact that CFBs are generally fairly evolved (MgO <8 wt. %) and contaminated by lithosphere, which can hinder the identification of their parental magma compositions and ultimate mantle sources (e.g., Jourdan et al. 2007a; Sano et al. 2001; Tommasini et al. 2005; Wooden et al. 1993). Some recent studies have suggested that pyroxenitic or "refertilized" mantle components, generated by the recycling of crustal materials back into the mantle, can be an important source component in CFB parental magmas (Gibson, 2002; Sobolev et al., 2007; Tuff et al., 2005).

Some rare and primitive (MgO > 10 wt. %) rock types (picrites) show geochemical affinity to sublithospheric mantle sources and are crucial in understanding the mantle sources of the largest CFB provinces (e.g., Gibson et al., 2000; Heinonen et al., 2010; Lightfoot et al., 1993; Peate et al., 2003; Riley et al., 2005; Storey et al., 1997). Mineral chemistry of these primitive rocks has widely been used to estimate the composition of their primary melts and the mineral composition and thermodynamical properties of their mantle sources (e.g., Heinonen and Luttinen, 2008; Larsen and Pedersen, 2000; Sobolev et al., 2007; Thompson and Gibson, 2000).

The Jurassic (~180 Ma) Karoo large igneous province (LIP) was formed during the initial stages of break-up of the Gondwana supercontinent (Fig. 1). It is a typical CFB province in that the majority of the rocks are basalts that are characterized by geochemical affinity to

ACCEPTED MANUSCRIPT

subcontinental lithospheric mantle (SCLM) and show evidence of variable degrees of contamination by the continental crust (e.g., Hawkesworth et al., 1984; Jourdan et al., 2007a; Luttinen et al., 1998; Sweeney et al., 1994). In the Antarctic segment of the Karoo LIP (Fig. 1), however, some primitive and nearly uncontaminated dike suites of sublithospheric geochemical character have been described (Heinonen and Luttinen, 2008; Heinonen et al., 2010; Luttinen and Furnes, 2000; Luttinen et al., 1998; Riley et al., 2005). At Ahlmannryggen, basaltic and picritic dikes crosscut the local Precambrian basement and have been sub-divided into four distinct geochemical groups (Groups 1–4; Riley et al., 2005). Two of the groups (3 and 4) include a subset of samples with MgO > 12 wt. % (Harris et al., 1991; Riley et al., 2005). High-Fe (FeO_{tot} up to 14 wt. %) Group 3 dikes lack a notable lithospheric overprint and show a depleted mantle -like ε_{Nd} (from +5 to +9 at 180 Ma), whereas Group 4 shows more enriched incompatible-trace-element and isotopic signatures (e.g., ε_{Nd} = from -4.6 to +2.4 at 180 Ma) that may reflect the mixing of melts from both asthenospheric and lithospheric sources (Riley et al., 2005).

In order to estimate the primary melt compositions and the mantle sources of the Ahlmannryggen Group 3 and 4 dikes, we have performed a comprehensive mineral chemical analysis (~800 data points) on them. Most of the samples are relatively fresh and therefore suitable for such an approach. In addition, the variable mineral composition, including orthopyroxene as a phenocryst and groundmass phase, enables us to place constraints on the pressures of crystallization and depth of emplacement of the dikes.

2. Geological setting

2.1. Bedrock of western Dronning Maud Land

The bedrock of western Dronning Maud Land comprises igneous, sedimentary, and metamorphic rock types that range in age from Archean to Mesozoic (Wolmarans and Kent, 1982). The

ACCEPTED MANUSCRIPT

Jurassic Karoo CFBs are exposed at Vestfjella, Kirwanveggen, and Heimefrontfjella, and represent the uppermost stratigraphic unit (Fig. 1). Associated dikes that crosscut the local basement are more widespread and can also be found at Ahlmannryggen, Mannefallknausane, and H. U. Sverdrupfjella (Fig. 1). Below the CFBs, late Paleozoic sediments are known to sporadically overlie the Precambrian basement at Vestfjella, Heimefrontfjella, and southwest Kirwanveggen (e.g., Juckes, 1972; Wolmarans and Kent, 1982). The Precambrian basement of the area can be divided into the Archean Grunehogna craton and the Mesoproterozoic Maud Belt (Fig. 1) that, respectively, were juxtaposed with the temporally and spatially related Kalahari craton and Namaqua-Natal metamorphic belts of southern Africa prior to the Jurassic break-up of the Gondwana supercontinent (e.g., Jacobs et al., 1993, 2003, 2008).The Maud Belt is dominated by ortho- and paragneisses that are largely the result of high-grade metamorphism and deformation of a volcanic arc during the Grenville-age assembly of the Rodinia supercontinent ~1.1 Ga ago (e.g., Groenewald et al., 1995; Grosch et al., 2007; Jacobs et al., 1993, 2003). The Archean craton is only exposed at Annandagstoppane (Fig. 1) (Barton et al., 1987; Marschall et al., 2010) and is elsewhere covered by Mesoproterozoic (≥1.1 Ga) Ritscherflya Supergroup supracrustal rocks (Wolmarans and Kent, 1982) and/or by large mafic intrusions of the Borgmassivet Intrusives (Krynauw et al., 1988, 1991) that probably intruded the supracrustal rocks shortly after their burial (Curtis and Riley, 2003; Krynauw et al., 1988).

2.2. The Karoo CFB province and associated primitive rocks

The Karoo CFBs were generated in a developing rift between the continents of Africa and Antarctica, both then part of the Gondwana supercontinent (Fig. 1), with the main phase of magmatism taking place in the interval 184–178 Ma ago (Jourdan et al., 2005). The bulk of the flood basalts (original volume estimated at ~$2 \cdot 10^6$ km^3; Richards et al., 1989) are exposed in southern Africa, where the majority of the lavas and associated intrusive rocks are basalts (MgO ≤ 8 wt. %) that show strong geochemical affinity to SCLM (e.g., Cox and Bristow, 1984; Hawkesworth et al. 1984; Jourdan et al. 2007a; Sweeney et al. 1994). The most primitive lavas

ACCEPTED MANUSCRIPT

are the Mwenezi picrites (Fig. 1), but even they exhibit lithosphere-influenced geochemical signatures (Ellam, 2006; Ellam and Cox, 1989, 1991; Ellam et al., 1992; Sweeney et al., 1991). The only African Karoo CFBs that show geochemical affinity to sublithospheric mantle sources are some of the Rooi Rand E-MORB-type basaltic dikes (Fig. 1) that post-date the main magmatic phase by at least 5 Myr and may be related to the initial opening of the Indian Ocean (Duncan et al., 1990; Jourdan et al., 2007b).

Although the Antarctic Karoo flood basalts are also characterized by a lithospheric geochemical signature (e.g., Harris et al., 1990; Luttinen and Furnes, 2000; Luttinen et al., 1998, 2010), some of the dike rocks in the area show more unusual compositions (Table 1). The Group 3 and Group 4 picritic dikes of Ahlmannryggen (Fig. 1) have initially been described by Harris et al. (1991) and Riley et al. (2005). They crosscut the Precambrian metasupracrustal rocks of the Ritscherflya Supergroup, are 0.1–4.5 m wide, and strike ENE-WSW (Group 3) and NNE-SSW (Group 4). One 0.5 m wide Group 4 dike is also known from Kirwanveggen (Fig. 1). The Group 3 dikes show high concentrations of MgO (8–22 wt. %), FeO_{tot} (11–14 wt. %; Fig. 2b), and TiO_2 (3.3–4.9 wt. %; Fig. 2a), and low CaO (8–11 wt. %) (Table 1). Their trace element pattern is characterized by MORB-like Nb/Y (0.1–0.3), and La/Sm (0.8–1.3), and moderate Sm/Yb (3.0–3.8) (Fig. 2c). Isotopically, the rocks exhibit depleted mantle –like radiogenic Nd (ε_{Nd} from +5 to +9) and unradiogenic to slightly radiogenic Sr ($^{87}Sr/^{86}Sr$ = 0.7035–0.7062) at 180 Ma (Fig. 2d). Relative to Group 3, the Group 4 dikes show slightly lower MgO (6–16 wt. %) and FeO_{tot} (9–13 wt. %; Fig. 2b), similarly low CaO (8–10 wt. %), but slightly higher TiO_2 (4.0–5.5 wt. %; Fig. 2a) (Table 1). They exhibit Nb/Y (0.6–0.9) similar to oceanic island basalts (OIBs) and notable enrichment of LREE relative to HREE (La/Sm = 2.1–3.9, Sm/Yb = 3.7–7.7) (Fig. 2c). They are isotopically more enriched than Group 3 dikes in general by having ε_{Nd} from -5 to +2 and $^{87}Sr/^{86}Sr$ of 0.7048–0.7059 at 180 Ma (Fig. 2d). In both groups, the samples with relatively lower initial ε_{Nd} and higher initial ε_{Sr} show evidence of subtle contamination with continental crust (e.g., by having higher Th/Ta relative to the other samples of the same group; cf. Fig. 2c). Ar-Ar whole-rock plateau ages of 187.3 ± 3.6 Ma (Group 3) and 178.3 ± 3.7 Ma (Group 4) are within-

ACCEPTED MANUSCRIPT

error from the Karoo main phase, but the plateaus are significantly disturbed and comprise only 50–60% of the total argon released (Riley et al., 2005).

In addition to Ahlmannryggen, two distinct geochemical types of unusual high Mg-Fe dikes (MgO > 12 wt. %; FeO_{tot}> 14 wt. %) have been described from Vestfjella (Heinonen and Luttinen, 2008). The depleted ferropicrite suite (La/Sm = 1.8–2.3, Sm/Yb = 2.9–4.2, Nb/Y = 0.3–0.5, initial ε_{Nd} from +4 to +8, and $^{87}Sr/^{86}Sr$ = 0.7030–0.7036 at 180 Ma; Fig. 2c, d) that includes basalts, ferropicrites, and meimechites has been ascribed to ambient sublithospheric peridotite sources as it is isotopically indistinguishable from the MORBs of Southwest Indian Ridge (SWIR), the present day manifestation of the Mesozoic Africa-Antarctica rift. In comparison, the enriched ferropicrite suite exhibit OIB-like trace element and isotopic characteristics (La/Sm = 2.4–2.8, Sm/Yb = 4.5–5.0, Nb/Y = 0.6–0.8, initial ε_{Nd} from +2 to +4, and $^{87}Sr/^{86}Sr$ = 0.7043–0.7050 at 180 Ma; Fig. 2c, d) indicative of pyroxenite sources (Heinonen et al., 2010). Notable differences in major element, trace element, and isotopic signatures suggests that the primitive Ahlmannryggen and Vestfjella dikes do not have a direct petrogenetic relationship (Heinonen and Luttinen, 2008; Riley et al., 2005; cf. Fig. 2).

3. Sample selection and analytical techniques

Twelve Group 3 and Group 4 samples that showed the least evidence of hydrothermal alteration were selected for mineral chemical analysis: these included four basaltic (MgO = 9–12 wt. %; Z1803.1, Z1803.3, Z1803.5, and Z1812.3) and four picritic (MgO = 13–22 wt. %; Z1812.1, Z1813.1, Z1816.3, and Z1817.2) dike samples from Group 3, and one basaltic (MgO = 12 wt. %; Z1825.3) and three picritic (MgO = 14–17 wt. %; Z1826.1, Z1826.2, and Z1838.1) dike samples from Group 4. The major element geochemical characteristics of the samples are presented in Table 1. All samples have been collected close to the chilled margin of the host dike.

Mineral compositions were determined at the Geological Survey of Finland (GTK) with a Cameca SX-100 electron probe micro-analyzer (EPMA) equipped with five wavelength-

ACCEPTED MANUSCRIPT

dispersive spectrometers, and at the Department of Geosciences and Geography (DGG), University of Helsinki, with a JEOL JXA-8600 EPMA equipped with four wavelength-dispersive spectrometers. The instrument at DGG was specifically used for back-scattered electron (BSE) imaging and to study chemical variation in profiles across olivine and pyroxene phenocrysts. Matrix corrections were performed with the Cameca Peak Sight software using the φρz correction at GTK and with the XMAS analysis software using the PAP correction at the DGG. Both microprobes were calibrated with a combination of natural and synthetic oxide and silicate standards. In the case of V, an element standard was used at DGG. The acceleration voltage, sample current, and beam diameter for the analyses were 20 kV, 20 nA, and 4 μm at GTK, and 20 kV, 15 nA, and 10 μm at DGG, respectively. Total peak count times were 190 seconds in the case of GTK and 185 seconds in the case of DGG (see Electronic Appendix A for element-specific peak and background count times). The precisions of the methods were evaluated by performing repeated analyses on natural standard materials: the coefficient of variation was below 1 % for major-element oxides (> 10 wt. %) in both laboratories, below 5 % at GTK and below 2% at DGG for minor-element oxides (1–10 wt. %), and below 10 % at GTK and below 15% at DGG for trace-element oxides (0.1–1.0 wt. %).

Additional Fe-Mg data on 200 olivine phenocrysts were acquired with a scanning electron microscope (SEM) JEOL JSM5900LV that is equipped with an energy-dispersive spectrometer at GTK. Although the instrument is not calibrated with standards, our analysis of 72 Cameca SX-100 duplicate points from olivine shows that the method reproduces the olivine Fo contents with an average discrepancy of only -0.1 Fo units (1σ error = 0.8 Fo units) and R^2 of 0.95. Additional SEM data was used only to produce a more representative dataset of the olivine Fo composition.

The complete dataset (~ 200 SEM and ~600 EPMA data points) and a more detailed review of the analytical methods are available in the Electronic Appendix A.

4. Petrography and mineral chemistry

ACCEPTED MANUSCRIPT

The petrography of the samples is summarized in Table 2 and some specific features and mineral compositions of the two different groups are summarized in the following text. All the samples analyzed in this study are porphyritic (often glomeroporphyritic) with euhedral to subhedral olivine (or olivine pseudomorphs) and/or pyroxene phenocrysts (that contain Cr-spinel and groundmass inclusions) surrounded by micro- to cryptocrystalline groundmass consisting of pyroxene, plagioclase, and Fe-Ti oxides (Fig. 3). One of the most conspicuous features is that orthopyroxene is a more common phenocryst phase than clinopyroxene (augite) and is sometimes also found in the groundmass. Orthopyroxene is rare in Karoo CFBs in general and has only been found as phenocrysts in some primitive lavas (e.g., Cox and Jamieson, 1974; Luttinen and Siivola, 1997) and dikes (e.g., Neumann et al., 2011). .

4.1. Group 3

In Group 3 samples, olivine (or its pseudomorphs; Ø ≤ 2.0 mm; 2–12 vol. %) and orthopyroxene (Ø ≤ 4 mm; 0–18 vol. %; invariably mantled by clinopyroxene) are the most common phenocryst phases. The groundmass, when optically identifiable, generally consists of pyroxenes (≤ 47 vol. %), plagioclase (≤ 35 vol. %), and Fe-Ti oxides (≤ 26 vol. %). Samples Z1803.1 and Z1803.5 are exceptional as they do not contain orthopyroxene phenocrysts, but microphenocrysts of olivine (Ø ≤ 1 mm; 3–8 wt. %) and augite (Ø ≤ 0.5 mm; 12–13 vol. %) ± plagioclase (c-axis < 2 mm; 0–1 vol. %) surrounded by a micro- to cryptocrystalline groundmass in which Fe-Ti oxides show dendritic quench growth textures. Quartz/carbonate-filled amygdules are rare.

4.1.1. Olivine

Samples Z1803.1, Z1803.5, Z1813.1, Z1817.2, and Z1816.3 contain fresh olivine phenocrysts that are relatively homogeneous in composition apart from thin (≤ 0.2 mm) relatively more Fe-rich rims. Olivine core Fo contents of individual samples vary between 79–82 (2σ = 2–3) mol. % on average; a notable exception are the two highly magnesian phenocrysts ($Fo_{89–90}$) found in sample Z1816.3 (mean $Fo_{82\pm2}$ with high-Mg olivines excluded) (Fig. 4). Olivine phenocrysts in

ACCEPTED MANUSCRIPT

sample Z1803.1 are in or close to being in equilibrium with the whole-rock composition, whereas other Group 3 samples show evidence of olivine accumulation by having higher whole-rock Mg# than excepted for olivine-liquid equilibrium (Fig. 4). All olivines have high CaO contents (≥ 0.16 wt. %) indicating that they are not mantle xenocrysts (cf. Simkin and Smith, 1970). NiO contents of the Group 3 olivines exhibit notable variation between samples (Fig. 5): at a given Fo content samples Z1803.1 and Z1803.5 have ~20% higher olivine NiO contents on average (0.51 wt. % at $Fo_{82,}$ calculated by assuming linear Fo-NiO trend) than samples Z1813.1 and Z1816.3 (0.43 and 0.42 wt. % at Fo_{82}, respectively). Olivines from sample Z1817.2 plot in between these two groups (0.47 wt. % at Fo_{82}).

4.1.2. Pyroxenes

Augite-mantled orthopyroxene is mainly found as phenocrysts, but in samples Z1812.1 and Z1812.3 it is also found in the groundmass. Samples Z1803.1 and Z1803.5 do not contain orthopyroxene at all. In the other samples, we have identified three different types of orthopyroxene phenocrysts: 1) Phenocrysts with thick (up to 0.5 mm) augite rims that host orthopyroxene inclusions. In some smaller phenocrysts augite dominates so that only small irregular orthopyroxene inclusions remain (samples Z1803.3 and Z1817.2; Fig. 3b); 2) Phenocrysts that exhibit thin (< 0.2 mm) augite rims and show notable oscillatory zoning (samples Z1812.1 and Z1812.3; Fig. 3c, d); 3) Phenocrysts that exhibit thin irregularly shaped augite rims (< 0.2 mm) and are not distinctively zoned (Z1813.1 and Z1816.3; Fig. 3e, f). Thin augite dissolution lamellae can be found in all types. All orthopyroxenes exhibit rather high Mg# (75–87; Fig. 6) and CaO (1–3 wt. %) and some of the analyzed crystals plot in the "pigeonite" field in the En-Fs-Ws ternary diagram (Fig. 7). Orthopyroxene phenocrysts in samples Z1803.3, Z1813.1, and Z1817.2 show compositions that plot close to the orthopyroxene-liquid equilibrium curve of $K_d(Fe^{2+}–Mg)^{opx\text{-}liq} = 0.35$ in Fig. 6.

Augite with CaO = 11–19 wt. % and Mg# = 64–83 is found in all samples as a groundmass phase, in samples Z1803.1, Z1803.5, and Z1817.2 as (micro)phenocrysts, and in

ACCEPTED MANUSCRIPT

samples Z1803.3, Z1812.1, Z1812.3, Z1813.1, Z1816.3, and Z.1817.2 as rims around and dissolution lamellae within orthopyroxene phenocrysts.

4.1.3. Cr-spinel

Cr-spinel is found as anhedral to euhedral inclusions in olivine and sometimes in pyroxene phenocrysts and rarely as small individual crystals (Ø ≤ 0.1 mm) in the groundmass. The compositional characteristics of the Cr-spinels can be summarized as follows: Cr_2O_3= 29–42 wt. % (Cr# = 70–78), MgO = 4–10 wt. % (Mg# = 17–45), FeO_{tot} = 31–48 wt. %, Al_2O_3= 7–11 wt. %, and TiO_2 = 4–8 wt. %. Cr# and Mg# show positive correlation with the host olivine Fo content. All the Group 3 spinels plot within or close to the LIP spinel field in the discrimination diagram of Kamenetsky et al. (2001) (Fig. 8).

4.2. Group 4

All four Group 4 samples contain olivine phenocrysts (Ø ≤ 2.0 mm; 4–28 vol. %) and, except in the case of Z1838.1, also orthopyroxene phenocrysts (Ø ≤ 2.5 mm; 2–4 vol. %) (Fig. 3a). The phenocrysts are surrounded by a micro- to cryptocrystalline (acicular pyroxene and dendritic Fe-Ti oxides) and partially glassy groundmass. Sample Z1838.1 contains ~1 vol. % of quartz/carbonate-filled small amygdules (Ø ≤ 0.5 mm), which are otherwise rare.

4.2.1. Olivine

Whereas sample Z1825.3 ($Fo_{85\pm2}$; average ± 2σ) and Z1838.1 ($Fo_{87\pm2}$) exhibit relatively homogeneous olivine populations, sample Z1826.1 ($Fo_{85\pm5}$; two populations may be distinguished at $Fo_{83\pm3}$ and $Fo_{88\pm2}$) and Z1826.2 ($Fo_{86\pm5}$) show a spectrum of petrographic and compositional characteristics between two end-member types: 1) comparatively small phenocrysts with low Fo contents (< Fo_{86} in general) and homogeneous Fo distribution (except for the thin Fe-rich rims), and 2) larger phenocrysts that show normal or oscillatory progressive zoning ranging from relatively Mg-rich (up to Fo_{90}) to Fe-rich (down to Fo_{81}) compositions (Fig.

ACCEPTED MANUSCRIPT

3g, h; Fig. 4). Olivine phenocrysts in sample Z1825.3 are in or close to being in equilibrium with the whole-rock composition (Fig. 4). Akin to Group 3 olivines, all Group 4 olivines exhibit high CaO contents (≥ 0.15 wt. %) indicative of a phenocrystic origin (cf. Simkin and Smith, 1970). Average NiO content of the Group 4 olivines (0.32 wt. % at $Fo_{80–81}$), however, is lower at a given Fo content compared to Group 3 olivines (0.39–0.46 wt. % at $Fo_{80–81}$) (Fig. 5).

4.2.2. Pyroxenes

Orthopyroxene phenocrysts found in samples Z1825.3, Z1826.1, and Z1826.2 are weakly zoned, have thin (< 0.2 mm) augite rims, contain augite dissolution lamellae, are homogeneous in composition (Mg# = 83–86), and exhibit high CaO (2–4 wt. %). Orthopyroxene in sample Z1825.3 is in or close to being in equilibrium with the whole-rock composition (Fig. 6).

Augite (CaO = 11–19 wt. %) in the groundmass and in the rims of orthopyroxene phenocrysts shows a much wider compositional variation (e.g., Mg# = 63–83). With the exception of sample Z1838.1, the largest groundmass pyroxenes exhibit Ca-poor cores (Mg# = 83–86).

4.2.3. Cr-spinel

Similarly to Group 3 samples, Cr-spinel is commonly found as inclusions in olivine and is sometimes found as inclusions in pyroxene phenocrysts and/or in the groundmass. Relative to Group 3 spinels, the Group 4 spinels exhibit higher Cr_2O_3 (43–50 wt. %; Cr# = 81–85), similar MgO (7–10 wt. %; Mg# = 34–48) and TiO_2 (4–5 wt. %), and lower FeO_{tot} (27–35 wt. %) and Al_2O_3 (6–7 wt. %). All Group 4 spinels plot in the LIP spinel field in the discrimination diagram of Kamenetsky et al. (2001) (Fig. 8).

5. Constraints on magma differentiation

5.1. Evidence for magma mixing and recognition of near-melt compositions

ACCEPTED MANUSCRIPT

The textural and mineral chemical characteristics of the Ahlmannryggen Group 3 and 4 dikes (Fig. 3, 4, 6) enable us to explore the differentiation history of their parental magmas and to filter out the whole-rock compositions that are not likely to represent near-melt compositions. Some compositional characteristics, for example the relative Fe-enrichment of Group 3 samples (Fig. 2b), could result from mixing of evolved and primitive magmas or from crystal accumulation (cf. Heinonen and Luttinen, 2008).

The Group 3 samples exhibit relatively uniform olivine core compositions (average $Fo_{79–82}$; $2\sigma = 2–3$ mol. %), apart from samples Z1816.3 and Z1817.2 which contain few anomalously Mg-rich ($Fo_{86–90}$) olivine phenocrysts (Fig. 4). Most of these Mg-rich olivines exhibit the characteristic high NiO of Group 3 magmas (Fig. 5) and thus are not likely to represent trapped "xenocrysts" from other magmatic lineages (e.g., Group 4). Apart from the thin Fe-rich rims, they do not exhibit compositional zoning and may represent crystals entrained into ascending magmas from earlier high-Mg cumulates. The lack of thick progressive zoning indicates that the Group 3 high-Mg olivines were not in prolonged contact with the host magma and this excludes their origin as early-stage precipitates in a dynamic Fe-depleted melting column (cf. Keiding et al., 2011). Pyroxene, which responds to changing conditions slower than olivine (cf. Streck, 2008), shows considerable textural and compositional variation in Group 3 samples. The replacement of orthopyroxene by augite in samples Z1803.3 and Z1817.2 (Fig. 3b) is most readily attributed to decreasing pressure, i.e., ascent of the crystallizing magma (cf. section 5.2.). Combined, the thickness of the concentric bands (> 10 μm) and the correlation of Mg# with Cr_2O_3 (Fig. 3d) in orthopyroxene phenocrysts of samples Z1812.1 and Z1812.3 infer that the zoning is likely to reflect dynamic magma mixing rather than kinetics on the solid-liquid interface or changes in oxygen fugacity (cf. Streck, 2008).

The continuous compositional range of olivines from Fo_{90} to Fo_{79} (also showing linear patterns of NiO and CaO) in Group 4 samples (Fig. 4, 5) implies that these olivines record a continuous crystallization history of a primitive magma system. Some mixing of magmas took place, however, as indicated by the zoned olivine phenocrysts and bimodal olivine distribution in

ACCEPTED MANUSCRIPT

sample Z1826.1 (Fig. 3g, h; Fig. 4). Since olivine is known to respond rapidly to non-equilibrium conditions (cf. Streck, 2008), the gradational zoning of some of the most Mg-rich olivines is most likely to result from diffusive re-equilibration of distinct Mg-rich (~Fo_{87}) and Mg-poor (~Fo_{82}) zones subsequent to mixing (cf. O'Brien et al., 1988). Pyroxenes in the Group 4 samples do not exhibit significant zoning and indicate that the mixed magmas had olivine as a sole liquidus silicate phase.

Identifying samples that are likely to represent near-melt compositions is an essential prerequisite in modeling the primary melt compositions and mantle sources involved. Most of the samples are not likely to represent near-melt compositions based on textural evidence (samples Z1812.1, Z1812.3, Z1826.1, and Z1826.2; cf. Fig. 3c, g) and the significant Fe-Mg disequilibrium between the whole-rock and olivine (samples Z1803.5, Z1813.1, Z1816.3, Z1817.2, Z1826.1, Z1826.2, and Z1838.1; Fig. 4) and/or pyroxene (samples Z1812.1, Z1812.3, Z1826.1, Z1826.2, and Z1816.3; Fig. 6). These features indicate that magma mixing and/or crystal accumulation took place in the evolution of most of the parental magmas. Two samples may closely correspond to melt compositions, however: olivine in sample Z1803.1 (Group 3) and olivine and orthopyroxene in sample Z1825.3 (Group 4) show a rather restricted compositional range and are in, or close to being in, equilibrium with the whole-rock composition (Fig. 4, 6). Furthermore, sample Z1803.1 is characterized by homogeneous olivine and augite microphenocrysts ($\leq$ 1 mm) that are likely to have crystallized close to emplacement depths, and sample Z1825.3 has a low phenocryst content (7 vol. %) (Table 2). Therefore, we suggest that the whole-rock compositions of Z1803.1 and Z1825.3 closely correspond to melt compositions. Importantly, the fact that sample Z1803.1 shows high FeO_{tot} (13 wt. %) demonstrates that the Fe-enrichment is an intrinsic feature of Group 3 magmas and not caused by Fe-rich olivine accumulation (cf. Heinonen and Luttinen, 2008).

In order to obtain further constraints on parental magma compositions, we performed phenocryst-subtraction calculations on cumulate samples Z1813.1 (Group 3) and Z1838.1 (Group 4) that show a rather restricted range of olivine composition and no textural evidence of magma mixing. We subtracted average phenocryst compositions in proportions suggested by

ACCEPTED MANUSCRIPT

petrography (5 wt. % of Fo_{82} olivine and 2 wt. % of orthopyroxene with Mg# of 84 from sample Z1813.1 and 9 wt. % of Fo_{87} olivine from sample Z1838.1) to reach average olivine-melt Mg-Fe equilibrium (Fig. 4). The hypothetical accumulation-corrected parental magma compositions of samples Z1813.1 and Z1838.1 are listed in Table 3.

5.2. Pressures of crystallization

The variable amount of olivine and pyroxenes as phenocrysts and in the groundmass of the samples Z1803.1 and Z1813.1 (Group 3) and samples Z1825.3, and Z1838.1 (Group 4) that are close representatives of melt compositions (Z1813.1 and Z1838.1 after accumulation correction, cf. previous section) enables us to place constraints on the pressures of crystallization. The observed variation in the groundmass (i.e., *in situ*) mineral composition is especially important as it enables us to estimate the emplacement depths of the dikes and the current erosion level of the Ahlmannryggen area. Our approach is largely based on the stability of orthopyroxene that is relatively sensitive to changes in pressure (e.g., O'Hara 1968), but also to the H_2O content of the melt (e.g., Feig et al., 2006). The discussion below is founded on the following observations.: 1) Orthopyroxene is not present in Group 3 sample Z1803.1; 2) Orthopyroxene is found as phenocrysts, but not as a groundmass phase, in Group 3 sample Z1813.1; 3) Orthopyroxene is found as a phenocryst *and* a groundmass phase in Group 4 sample Z1825.3; 4) Orthopyroxene is not found in Group 4 sample Z1838.1.

The parental magma compositions were modeled at variable crustal pressures (up to 10 kbar) using PELE software (Boudreau, 1999; version 7.07 published in 2010) that is based on the MELTS algorithm (Ghiorso and Sack, 1995). Oxygen fugacity (fO_2) was estimated to be one log unit below the quartz-fayalite-magnetite (QFM) buffer (cf. Frost, 1991) on the basis of spinel chemistry that indicates melt Fe^{3+}/Fe_{tot} values of 0.10 ± 0.03 (2σ) for Group 3 and 0.08 ± 0.04 for Group 4 (calculated with equations of Maurel and Maurel, 1982). The rarity of amygdules in most of the samples and the absence of primary magmatic hydrous minerals as phenocryst or groundmass phases or within crystallized melt inclusions indicate that the parental magmas were

ACCEPTED MANUSCRIPT

not significantly enriched in volatiles and support a H_2O-poor (< 1.0 wt. %) nature for them (cf. Heinonen and Luttinen, 2010); minimum value of H_2O^{liq} = 0.25 wt. % was chosen for the modeling as clinopyroxene does not crystallize prior to orthopyroxene from Z1803.1 parental magma at lower H_2O^{liq} contents (Fig. 9). Sample Z1838.1 is exceptional as it contains ~1 vol. % of amygdules and is the most enriched in several fluid-compatible elements (e.g., Ba and Rb), and also shows the highest calculated melt Fe^{3+}/Fe_{tot} ratio (0.12) of Group 4 samples. These characteristics could indicate higher H_2O content (~1 wt. %) in the parental magma compared to other samples in this study (cf. Gaillard et al., 2003). Accordingly, the PELE models were ran in a H_2O^{liq} range of 0.25–1 wt. %.

The PELE models ran in pressures of > 6 kbar do not correspond to groundmass petrography of the samples and thus only results in the pressure range of 0.5–6.0 kbar are compiled in Fig. 9. It should be kept in mind that different ages have been suggested for the Group 3 (~190 Ma) and Group 4 (~178 Ma) dikes (Riley et al., 2005). Because the thickness of the Karoo lava pile could have been several kilometers less and crustal pressures several kbars lower during the crystallization of the Group 3 dikes, the results of the two groups must be interpreted separately.

In the case of Group 3, sample Z1803.1 shows a crystallization sequence with augite preceding plagioclase without orthopyroxene (Table 2), which is only possible when $H_2O^{liq} \geq$ 0.25 wt. % and the pressure is below 5 kbar. Given that the H_2O^{liq} contents of Group 3 parental magmas were unlikely to be as high as 1 wt. %, the crystallization of the sample Z1803.1 without orthopyroxene took place within a pressure range of 2.0–5.0 kbar (Fig. 9), which corresponds to crustal depths of 7–18 km. At least some of the Group 3 magmas crystallized orthopyroxene already at deeper crustal levels at pressures of ≥ 6 kbar (≥ 20 km) as indicated by the presence of orthopyroxene phenocrysts in sample Z1813.1 (not shown in Fig. 9).

In the case of Group 4, at pressures of 3.0–5.0 kbar, melt corresponding to sample Z1825.3 crystallizes orthopyroxene before augite when H_2O^{liq} = 0.25–0.75 wt. %, and orthopyroxene does not crystallize from the Z1838.2 parental magma when H_2O^{liq} = 0.50–1.00 wt. % (Fig. 9). Pressures of 3.0–5.0 kbar correspond to crustal depths of 9–18 km and we suggest that the

ACCEPTED MANUSCRIPT

emplacement of the Group 4 dikes took place within such depth range during the late stages of Karoo magmatism.

In comparison, the crystallization of orthopyroxene phenocrysts in Mwenezi picrites (Fig. 7) has been estimated to have taken place at pressures of 6–12 kbar. The potassic nature of the Mwenezi picrites (K_2O = 1–3 wt. %) increases the stability of olivine at the expense of orthopyroxene (Cox and Jamieson, 1974) and may explain the higher pressures relative to the low-K Ahlmannryggen samples (cf. Table 1).

The presence of orthopyroxene as a groundmass phase in Ahlmannryggen samples indicates a deep erosional level of the local basement. The closest exposure of extrusive Karoo basalts is located 150 km south at Kirwanveggen, on the southern side of the Pencksökket subglacial trough that represents a deeply eroded major fault line (e.g., Grantham and Hunter, 1991; Fig. 1). Given that the base of these flood basalts is exposed and that the maximum thickness of the lava succession was very unlikely more than ~10 kilometres (maximum Karoo lava pile thickness; Watkeys, 2002), Ahlmannryggen may have been vertically uplifted several kilometers relative to Kirwanveggen after the Karoo event. Such scales of crustal movement are not exceptional in active zones of crustal extension (e.g., Basin and Range; Egger and Miller, 2011).

6. Constraints on primary melts and mantle sources

The mantle sources of the Ahlmannryggen dikes have been discussed previously by Riley et al. (2005) on the basis of whole-rock major and trace element geochemistry, and their Sr and Nd isotopic composition. They suggested an Fe-enriched E-MORB or plume source for Group 3 and depleted mantle + lithospheric mantle source for Group 4. Since the Group 3 samples do not show geochemical evidence of significant lithospheric contamination, their mineral chemical characteristics enable us to estimate their primary melt compositions and place tighter constraints on the nature of their mantle source. We also follow the same treatment for Group 4 magmas,

ACCEPTED MANUSCRIPT

although in their case it is necessary to keep in mind the possibility of mixing of magmas from sublithospheric and lithospheric mantle sources (Riley et al., 2005).

6.1. Hypothetical primary melt modeling

In the absence of glassy samples, we have estimated primary melt compositions using conventional mixing calculations: phenocryst minerals are added to the whole-rock compositions until mineral-melt equilibrium with the most primitive phenocrysts of the dike groups is attained. To our knowledge, thermodynamic modeling programs (e.g., Herzberg and Asimow, 2008; Lee et al., 2009) are designed for peridotite-sourced melts and are thus unreliable in the case of Ahlmannryggen dikes due to the likelihood of pyroxenite source components (cf. section 7.2.). Since the thermodynamical properties of olivine are more tightly constrained and less variable than those of orthopyroxene, we focused on modeling the primary melts on the basis of olivine-liquid equilibrium (cf. Fig. 4, 6; Putirka, 2008).

We have used samples Z1803.1 (Group 3) and Z1825.3 (Group 4) as starting compositions in the modeling based on their likely correspondence to melt compositions (Fig. 4). The petrographic evidence suggests fractionation of two major minerals, olivine and orthopyroxene, from the parental magmas. In order to evaluate the significance of orthopyroxene fractionation, we used two extreme assemblages in the modeling: (1) Olivine phenocrysts are present in all samples and thus olivine-only fractionation is the primary option in both groups. (2) As an estimation of the possible maximum amount of pyroxene in the assemblage, we used 25% olivine and 75% orthopyroxene (Group 3) and 60% olivine and 40% orthopyroxene (Group 4) as indicated by the petrographic evidence (cf. Table 2). In the modeling, $(Fe^{3+}/Fe_{tot})^{liq}$ was considered to be 0.10 in the case of Group 3 and 0.08 in the case of Group 4 (cf. section 5.2), and $K_d(Fe^{2+}–Mg)^{ol\text{-}liq}$ was either 0.32 or 0.35 (Putirka, 2005; cf. Fig. 4). The most primitive olivines (used as an equilibrium olivine) in both groups are Fo_{90}; due to the scarcity of such primitive olivines in Group 3 samples, however, we also calculated Group 3 primary melts in equilibrium with Fo_{84} olivine (cf. Fig. 4).

ACCEPTED MANUSCRIPT

The hypothetical primary melts (group-specific end-members) are listed in Table 3. The Group 3 primary melts are picritic (MgO = 11–13 wt. %) to meimechitic (MgO = 18–22 wt. %) depending on the choice of equilibrium olivine and the Group 4 primary melts are just on the brink of picrite-meimechite division at MgO = 17–19 wt. % (cf. Le Bas, 2000). The main difference between the melts calculated with $K_d(Fe^{2+}–Mg)^{ol-liq}$ of 0.32 and 0.35 is the up to 3 wt. % higher MgO in the latter case. The most notable effect of including orthopyroxene in the fractionating assemblage is that the SiO_2 contents are 1–4 wt. % higher relative to primary melts calculated with addition of olivine only.

6.2. Mantle sources

Geochemical and mineral chemical features of primitive volcanic rocks reflect the mineral composition of their mantle sources. Relatively low CaO/MgO (Herzberg and Asimow, 2008; Fig. 10) and high Zn/Fe (Le Roux et al., 2010; Fig. 11b) whole-rock compositions and high Ni and low Mn contents in olivine phenocrysts (Sobolev et al., 2005; 2007; Fig. 11a) indicate derivation of the primary melts from pyroxene-rich sources. In addition, primitive volcanic rocks with TiO_2 > 2 wt. % are not likely to represent depleted or pyrolitic mantle peridotite-sourced partial melts (Prytulak and Elliott, 2007; Walter, 1998). It should be emphasized, however, that high pressures of melting and crystallization also increase olivine Ni (Li and Ripley, 2010) and Mn compatibility shows positive correlation with water activity in a garnet-bearing source (Balta et al., 2011). We focus our discussion on olivine NiO and whole-rock CaO/MgO and Zn/Fe; the Mn-in-olivine tracer is not used due to limited precision of the data (Qin and Humayun, 2008; Sobolev et al., 2007). Importantly, the high TiO_2 contents (> 3 wt. %) of the Group 3 and 4 dikes (Fig. 2a) indicate that a relatively more enriched source than depleted or pyrolitic mantle peridotite was required in both cases. In the following text, we use PX# (13.81 – 0.274*MgO – CaO) introduced by Herzberg and Asimow (2008) to define the nature of the source: negative values indicate relatively peridotite-rich sources whereas positive values indicate relatively pyroxenite-rich sources (cf. Fig. 10).

ACCEPTED MANUSCRIPT

Significant pyroxenite component for Group 3 magmas is indicated by high olivine Ni and high whole-rock Zn/Fe and PX# that resemble those of the Hawaiian shield tholeiites and the Vestfjella enriched ferropicrite suite, the sources of which have been interpreted to contain pyroxenite (Fig. 11; Heinonen and Luttinen, 2008; Heinonen et al., 2010; Herzberg, 2006; Sobolev et al., 2007). A more detailed examination of the geochemistry of the Group 3 dikes reveals that their origin was more complicated, however. First, Group 3 dikes show considerable variation in olivine NiO contents (Fig. 5) and positive correlation between olivine NiO and PX# (Fig. 11a). Given that they do not show evidence of significant lithospheric contamination (Riley et al., 2005; Fig. 2d) and exhibit a restricted range of Sm/Yb (3.0–3.8; Fig. 2c) compatible with melting at rather constant pressures, the variation in olivine NiO most likely reflects variation in the mantle source composition. In addition, none of the modeled olivine-orthopyroxene addition trends coincide with the geochemical trend of the Group 3 samples and most of the calculated primary melts have excessively high MgO and low CaO to be derived from either pyroxenite or peridotite mantle source (Fig. 10). These observations indicate that the compositional variation of Group 3 dikes cannot be explained by fractional crystallization of the observed phenocryst phases and that the calculated hypothetical primary melts are likely to be petrologically meaningless (and thus unsuitable for thermodynamical modeling).

Instead, we propose that the salient geochemical features of Group 3 dikes are associated with mixing of magmas derived from mixed pyroxenite-peridotite sources. We regard that the subset of Group 3 dikes that contain relatively Fe-rich olivine phenocrysts (~Fo_{80}; Fig. 4) and exhibit high olivine NiO and whole-rock PX# (e.g., sample Z1803.1) represent magmas with relatively high amount of pyroxenite source component (Fig. 10 and 11a). On the other hand, dikes that contain the most magnesian olivine (~Fo_{90}; Fig. 4), low olivine NiO, and low whole-rock PX# (e.g., cumulate sample Z1816.3) represent magmas with relatively high amount of peridotite source component (Fig. 10 and 11a). In fact, reducing the effect of phenocryst accumulation by stepwise removal of olivine (~10 %) and orthopyroxene (~12 %) from cumulate sample Z1816.3 yields a melt composition that plots into the peridotite partial melt field at MgO = 18 wt. % in Fig. 10. Although it is not possible to constrain the exact proportions of the

ACCEPTED MANUSCRIPT

different source components, the consistently high TiO_2 and Zn/Fe (Fig. 2a) imply involvement of pyroxenite sources in all Group 3 magmas.

Although the possibility of lithospheric contamination in the case of Group 4 dikes (Riley et al., 2005) hampers the identification of their initial mantle sources, they also show relatively high olivine NiO (although lower than in the case of Group 3), PX#, and Zn/Fe indicative of involvement of pyroxene-rich lithologies (Fig. 5 and 11). On the other hand, and as is the case in Group 3, the calculated primary melt compositions are relatively MgO-rich and indicate some contribution from peridotitic sources as well (Fig. 10). Mixing of Ca-rich peridotite partial melt (from lithospheric mantle?) with Ca-poor pyroxenite partial melt could hypothetically explain the combination of Fo_{90} phenocrysts and relatively Ca-poor and Ti-rich whole-rock composition of the Group 4 dikes.

Within the framework of the Karoo province, pyroxenite sources have been suggested for the lithosphere-signatured Mwenezi picrites (Sobolev et al., 2007) and the Vestfjella enriched ferropicrite suite (Heinonen and Luttinen, 2008; Heinonen et al., 2010), and we now propose them for Group 3 and Group 4 dikes of Ahlmannryggen. All of these pyroxenite-affinity high-Ti suites are geographically associated with the thick pre-breakup Gondwanan lithosphere (cf. Luttinen et al., 2010). Following Gibson (2002) and Sobolev et al. (2005), we propose that the thick lithosphere (> 200 km at present in Antarctica; Morelli and Danesi, 2004) limited high-degree melting of peridotite sources and led to predominance of melts from more fusible pyroxenite sources. In contrast, most of the low-Ti suites were likely generated within areas of thinned lithosphere (e.g., Luttinen et al. 2010). In such low-pressure environment, pyroxenite-derived melts are expected to become increasingly more diluted as a consequence of progressive melting of mantle peridotite (cf. Sobolev et al., 2005). It is important to note, however, that a predominant peridotite source component has also been identified in some of the Karoo high-Ti suites (e.g., the Vestfjella depleted ferropicrite suite; Heinonen and Luttinen, 2010; Heinonen et al., 2010).

In summary, the geochemical data for the two most likely uncontaminated Karoo CFB-related rock suites, the Group 3 dikes of Ahlmannryggen and the Vestfjella depleted ferropicrite

ACCEPTED MANUSCRIPT

suite, indicate involvement of sublithospheric pyroxenite and peridotite sources in Karoo magmatism. The nature of these sources (e.g., scales of heterogeneity and plume vs. upper mantle origin) and their relative contributions to Karoo high-Ti (and low-Ti) magmatism remain to be constrained (cf. Heinonen et al., 2010).

7. Conclusions

On the basis of the mineral chemistry and whole-rock geochemical data of the Ahlmannryggen Group 3 and Group 4 mafic and ultramafic dikes from the Antarctic extension of the Jurassic Karoo LIP, we present the following conclusions:

1. Group 3 and Group 4 dikes are characterized by Mg-rich olivine ($Fo_{76–90}$) and orthopyroxene (Mg# = 75–87) phenocrysts. Although most of the samples show textural and compositional evidence of phenocryst accumulation and/or magma mixing (e.g., by containing oscillatory zoned phenocrysts), some are void of mixing textures and the olivines in them are either in or close to Fe-Mg equilibrium with their respective host rocks.
2. Thermodynamical modeling based on the variable presence of two pyroxenes (orthopyroxene and clinopyroxene) indicates crystallization pressures of 2–5 kbar (depth of ~10–20 km) for the dikes.
3. Both groups show mineral chemical and geochemical evidence (high olivine NiO and whole-rock Zn/Fe and low whole-rock CaO) of derivation from pyroxenite sources. Furthermore, the uncontaminated Group 3 dikes show linear compositional characteristics that likely reflect variability in the mineral composition of the mantle source: dikes that contain the most Mg-rich olivine (~Fo_{90}) and exhibit relatively low olivine NiO and high whole-rock CaO derive from relatively pyroxene-poor sources, whereas samples with relatively Fe-rich olivine (~Fo_{80}), high olivine NiO, and low whole-rock CaO derive from relatively pyroxene-rich sources.

ACCEPTED MANUSCRIPT

4. Our study consolidates the view that pyroxenite-derived melts are more likely to be preserved in areas of thick continental lithosphere. All of the Karoo CFBs that show strong evidence of pyroxenite sources are high-Ti suites that were generated deeper in the mantle than the low-Ti suites.

Acknowledgements

The field and air operations staff at Halley Base during 2000–2001 are thanked for their support. Lassi Pakkanen and Bo Johanson are thanked for their generous support in using the instruments at GTK. Matti Poutiainen is thanked for technical support in using the point counter. Some of the diagrams have been produced with the help of the GCDkit software (Janoušek et al. 2006). Our research is funded by the Academy of Finland (Grant no. 252652).

References

Anderson, D.L., 1994. The sublithospheric mantle as the source of continental flood basalts: the case against the continental lithosphere and plume head reservoirs. Earth and Planetary Science Letters 123 (1-4), 269-280.

Anderson, D.L., 2005. Large igneous provinces, delamination, and fertile mantle. Elements 1, 271-275.

Balta, J.B., Asimow, P.D., Mosenfelder, J.L., 2011. Manganese partitioning during hydrous melting of peridotite. Geochimica et Cosmochimica Acta 75 (20), 5819-5833.

Barton, J.M.,Jr, Klemd, R., Allsopp, H.L., Auret, S.H., Copperthwaite, Y.E., 1987. The geology and geochronology of the Annandagstoppane granite, Western Dronning Maud Land, Antarctica. Contributions to Mineralogy and Petrology 97 (4), 488-496.

ACCEPTED MANUSCRIPT

Boudreau, A.E., 1999. PELE – a version of the MELTS software program for the PC platform. Computers & Geosciences 25 (2), 201-203. Version 7.07 of the software downloaded in 2010 from http://fds.duke.edu/db/Nicholas/eos/faculty/boudreau

Bryan, S.E., Ernst, R.E., 2008. Revised definition of large igneous provinces (LIPs). Earth-Science Reviews 86 (1-4), 175-202.

Campbell, I.H., 2005. Large igneous provinces and the mantle plume hypothesis. Elements 1, 265-269.

Campbell, I.H., Griffiths, R.W., 1990. Implications of mantle plume structure for the evolution of flood basalts. Earth and Planetary Science Letters 99 (1-2), 79-93.

Coltice, N., Phillips, B.R., Bertrand, H., Ricard, Y., Rey, P., 2007. Global warming of the mantle at the origin of flood basalts over supercontinents. Geology 35 (5), 391-394.

Corner, B., 1994. Geological evolution of western Dronning Maud Land within a Gondwana framework: Geophysics subprogramme. Final project report to SACAR. Department of Geophysics, Witwaterstrand University, South Africa, 21 pages.

Cox, K.G., Bristow, J.W., 1984. The Sabie River Basalt Formation of the Lebombo Monocline and South-east Zimbabwe. In: Erlank, A.J., (Ed.), Petrogenesis of the Volcanic Rocks of the Karoo Province. Geological Society of South Africa Special Publication 13, Johannesburg (ZAF), pp. 125-147.

Cox, K.G., Jamieson, B.G., 1974. The Olivine-rich Lavas of Nuanetsi: a Study of Polybaric Magmatic Evolution. Journal of Petrology 15 (2), 269-301.

Curtis, M.L., Riley, T.R., 2003. Mobilization of fluidized sediment during sill emplacement, western Dronning Maud Land, East Antarctica. Antarctic Science 15 (3), 393-398.

ACCEPTED MANUSCRIPT

Duncan, A.R., Armstrong, R.A., Erlank, A.J., Marsh, J.S., Watkins, R.T., 1990. MORB-related dolerites associated with the final phases of Karoo flood basalt volcanism in Southern Africa. In: Parker, A.J., Rickwood, P.C., Tucker, D.H. (Eds.), Mafic Dykes and Emplacement Mechanisms. Proceedings of the International Dyke Conference 2, Balkema, Rotterdam, pp. 119-129.

Egger, A.E., Miller, E.L., 2011.Evolution of the northwestern margin of the Basin and Range: The geology and extensional history of the Warner Range and environs, northeastern California. Geosphere 7 (3), 756-773.

Elkins-Tanton, L.T., 2005. Continental magmatism caused by lithospheric delamination. In: Foulger, G., Natland, J.H., Presnall, D.C., Anderson, D.L. (Eds.), Plates, Plumes, and Paradigms. Geological Society of America Special Paper 388, pp. 449-461.

Ellam, R.M., 2006. New constraints on the petrogenesis of the Nuanetsi picrite basalts from Pb and Hf isotope data. Earth and Planetary Science Letters 245 (1-2), 153-161.

Ellam, R.M., Cox, K.G., 1989. A Proterozoic lithospheric source for Karoo magmatism: evidence from the Nuanetsi picrites. Earth and Planetary Science Letters 92 (2), 207-218.

Ellam, R.M., Cox, K.G., 1991. An interpretation of Karoo picrite basalts in terms of interaction between asthenospheric magmas and the mantle lithosphere. Earth and Planetary Science Letters 105 (1-3), 330-342.

Ellam, R.M., Carlson, R.W., Shirey, S.B., 1992. Evidence from Re-Os isotopes for plume-lithosphere mixing in Karoo flood basalt genesis. Nature 359, 718-721.

Feig, S., Koepke, J., Snow, J., 2006.Effect of water on tholeiitic basalt phase equilibria: an experimental study under oxidizing conditions. Contributions to Mineralogy and Petrology 152 (5), 611-638.

ACCEPTED MANUSCRIPT

Frost, B.R., 1991. Introduction to oxygen fugacity and its petrologic importance. Reviews in Mineralogy and Geochemistry 25 (1), 1-9.

Gaillard, F., Pichavant, M., Scaillet, B., 2003.Experimental determination of activities of FeO and Fe2O3 components in hydrous silicic melts under oxidizing conditions. Geochimica et Cosmochimica Acta 67 (22), 4389-4409.

Ghiorso, M.S., Sack, R.O., 1995. Chemical mass transfer in magmatic processes IV. A revised and internally consistent thermodynamic model for the interpolation and extrapolation of liquid-solid equilibria in magmatic systems at elevated temperatures and pressures. Contributions to Mineralogy and Petrology 119 (2-3), 197-212.

Gibson, S.A., 2002. Major element heterogeneity in Archean to Recent mantle plume starting-heads. Earth and Planetary Science Letters 195 (1-2), 59-74.

Gibson, S.A., Thompson, R.N., Dickin, A.P., 2000. Ferropicrites: geochemical evidence for Fe-rich streaks in upwelling mantle plumes. Earth and Planetary Science Letters 174 (3-4), 355-374.

Grantham, G.H., Hunter, D.R., 1991. The timing and nature of faulting and jointing adjacent to the Pencksokket, western Dronning Maud Land, Antarctica. In: Thomson, M.R.A., Crame, J.A. and Thomson, J.W., (Eds.), Geological Evolution of Antarctica, Proceedings of the Fifth International Symposium on Antarctic Earth Sciences. Cambridge University Press, Cambridge, pp. 47-51.

Groenewald, P.B., Moyes, A.B., Grantham, G.H., Krynauw, J.R., 1995. East Antarctic crustal evolution: geological constraints and modelling in western Dronning Maud Land. Precambrian Research 75 (3-4), 231-250.

Grosch, E.G., Bisnath, A., Frimmel, H.E., Board, W.S., 2007. Geochemistry and tectonic setting of mafic rocks in western Dronning Maud Land, East Antarctica: implications for the geodynamic evolution of the Proterozoic Maud Belt. Journal of the Geological Society 164 (2), 465-475.

ACCEPTED MANUSCRIPT

Harris, C., Marsh, J.S., Duncan, A.R., Erlank, A.J., 1990. The petrogenesis of the Kirwan Basalts of Dronning Maud Land, Antarctica. Journal of Petrology 31 (2), 341-369.

Harris, C., Watters, B.R., Groenewald, P.B., 1991. Geochemistry of the Mesozoic regional basic dykes of western Dronning Maud Land, Antarctica. Contributions to Mineralogy and Petrology 107 (1), 100-111.

Hawkesworth, C.J., Marsh, J.S., Duncan, A.R., Erlank, A.J., Norry, M.J., 1984. The role of continental lithosphere in the generation of the Karoo volcanic rocks: evidence from combined Nd- and Sr-isotope studies. In: Erlank, A.J., (Ed.), Petrogenesis of the Volcanic Rocks of the Karoo Province. Geological Society of South Africa Special Publication 13, Johannesburg (ZAF), pp. 341-354.

Heinonen, J.S., Luttinen, A.V., 2008. Jurassic dikes of Vestfjella, western Dronning Maud Land, Antarctica: Geochemical tracing of ferropicrite sources. Lithos 105 (3-4), 347-364.

Heinonen, J.S., Luttinen, A.V., 2010. Mineral chemical evidence for extremely magnesian subalkaline melts from the Antarctic extension of the Karoo large igneous province. Mineralogy and Petrology 99 (3), 201-217.

Heinonen, J.S., Carlson, R.W., Luttinen, A.V., 2010. Isotopic (Sr, Nd, Pb, and Os) composition of highly magnesian dikes of Vestfjella, western Dronning Maud Land, Antarctica: A key to the origins of the Jurassic Karoo large igneous province? Chemical Geology 277 (3-4), 227-244.

Herzberg, C., 2006. Petrology and thermal structure of the Hawaiian plume from Mauna Kea volcano. Nature 444, 605-609.

Herzberg, C., Asimow, P.D., 2008. Petrology of some oceanic island basalts: PRIMELT2.XLS software for primary magma calculation. Geochemistry, Geophysics, Geosystems 9 (9), doi:10.1029/2008GC002057.

ACCEPTED MANUSCRIPT

Jacobs, J., Thomas, R.J., Weber, K., 1993. Accretion and indentation tectonics at the southern edge of the Kaapvaal Craton during the Kibaran (Grenville) Orogeny. Geology 21 (3), 203-206.

Jacobs, J., Bauer, W., Fanning, C.M., 2003. New age constraints for Grenville-age metamorphism in western central Dronning Maud Land (East Antarctica), and implications for the palaeogeography of Kalahari in Rodinia. International Journal of Earth Sciences 92 (3), 301-315.

Jacobs, J., Pisarevsky, S., Thomas, R.J., Becker, T., 2008.The Kalahari Craton during the assembly and dispersal of Rodinia. Precambrian Research 160 (1-2), 142-158.

Janoušek, V., Farrow, C.M., Erban, V., 2006. Interpretation of Whole-rock Geochemical Data in Igneous Geochemistry: Introducing Geochemical Data Toolkit (GCDkit). Journal of Petrology 47 (6), 1255-1259.

Jourdan, F., Féraud, G., Bertrand, H., Kampunzu, A.B., Tshoso, G., Watkeys, M.K., Le Gall, B., 2005. Karoo large igneous province: Brevity, origin, and relation to mass extinction questioned by new 40Ar/39Ar age data. Geology 33 (9), 745-748.

Jourdan, F., Bertrand, H., Schaerer, U., Blichert-Toft, J., Féraud, G., Kampunzu, A.B., 2007a.Major and trace element and Sr, Nd, Hf, and Pb isotope compositions of the Karoo large igneous province, Botswana-Zimbabwe: lithosphere vs mantle plume contribution. Journal of Petrology 48 (6), 1043-1077.

Jourdan, F., Féraud, G., Bertrand, H., Watkeys, M.K., 2007b. From flood basalts to the inception of oceanization: example from the 40Ar/39Ar high-resolution picture of the Karoo large igneous province. Geochemistry, Geophysics, Geosystems 8 (2), doi:10.1029/2006GC001392.

Juckes, L.M., 1972. The geology of north-eastern Heimefrontfjella, Dronning Maud Land.British Antarctic Survey, Scientific Report 65, 44 pages.

ACCEPTED MANUSCRIPT

Kamenetsky, V.S., Crawford, A.J., Meffre, S., 2001. Factors controlling chemistry of magmatic spinel: an empirical study of associated olivine, Cr-spinel and melt inclusions from primitive rocks. Journal of Petrology 42 (4), 655-671.

Keiding, J.K., Trumbull, R.B., Veksler, I.V., Jerram, D.A., 2011. On the significance of ultra-magnesian olivines in basaltic rocks. Geology 39 (12), 1095-1098.

Krynauw, J.R., Hunter, D.R., Wilson, A.H., 1988. Emplacement of sills into wet sediments at Grunehogna, western Dronning Maud Land, Antarctica. Journal of the Geological Society of London 145, 1019-1032.

Krynauw, J.R., Watters, B.R., Hunter, D.R., Wilson, A.H., 1991. A review of the field relations, petrology and geochemistry of the Borgmassivet intrusions in the Grunehogna Province, western Dronning Maud Land, Antarctica. In: Thomson, M.R.A., Crame, J.A. and Thomson, J.W., (Eds.), Geological Evolution of Antarctica, Proceedings of the Fifth International Symposium on Antarctic Earth Sciences. Cambridge University Press, pp. 33-39.

Larsen, L.M., Pedersen, A.K., 2000. Processes in high-Mg, high-T magmas: evidence from olivine, chromite and glass in Palaeogene picrites from West Greenland. Journal of Petrology 41 (7), 1071-1098.

Le Bas, M.J., 2000. IUGS reclassification of the high-Mg and picritic volcanic rocks. Journal of Petrology 41 (10), 1467-1470.

Le Roux, V., Lee, C.A., Turner, S.J., 2010. Zn/Fe systematics in mafic and ultramafic systems: implications for detecting major element heterogeneities in the Earth's mantle. Geochimica et Cosmochimica Acta 74 (9), 2779-2796.

LeRoux, V., Dasgupta, R., Lee, C.-.A., 2011. Mineralogical heterogeneities in the Earth's mantle: Constraints from Mn, Co, Ni and Zn partitioning during partial melting. Earth and Planetary Science Letters 307 (3-4), 395-408.

ACCEPTED MANUSCRIPT

Lee, C.A., Luffi, P., Plank, T., Dalton, H., Leeman, W.P., 2009. Constraints on the depths and temperatures of basaltic magma generation on Earth and other terrestrial planets using new thermobarometers for mafic magmas. Earth and Planetary Science Letters 279 (1-2), 20-33.

Li, C., Ripley, E.M., 2010. The relative effects of composition and temperature on olivine-liquid Ni partitioning: Statistical deconvolution and implications for petrologic modeling. Chemical Geology 275 (1-2), 99-104.

Lightfoot, P.C., Hawkesworth, C.J., Hergt, J.M., Naldrett, A.J., Gorbachev, N.S., Fedorenko, V.A., Doherty, W., 1993. Remobilisation of the continental lithosphere by a mantle plume: major-, trace-element, and Sr-, Nd-, and Pb-isotope evidence from picritic and tholeiitic lavas of the Noril'sk District, Siberian Trap, Russia. Contributions to Mineralogy and Petrology 114 (2), 171-188.

Luttinen, A.V., Furnes, H., 2000. Flood basalts of Vestfjella: Jurassic magmatism across an Archaean-Proterozoic lithospheric boundary in Dronning Maud Land, Antarctica. Journal of Petrology 41 (8), 1271-1305.

Luttinen, A.V., Siivola, J.U., 1997. Geochemical characteristics of Mesozoic lavas and dikes from Vestfjella, Dronning Maud Land: recognition of three distinct chemical types. In: Ricci, C.A. (Ed.), The Antarctic Region: Geological Evolution and Processes. Siena: Terra Antarctica Publications, Italy, pp. 495–503.

Luttinen, A.V., Rämö, O.T., Huhma, H., 1998. Neodymium and strontium isotopic and trace element composition of a Mesozoic CFB suite from Dronning Maud Land, Antarctica: Implications for lithosphere and asthenosphere contributions to Karoo magmatism. Geochimica et Cosmochimica Acta 62 (15), 2701-2714.

Luttinen, A.V., Leat, P.T., Furnes, H., 2010. Björnnutane and Sembberget basalt lavas and the geochemical provinciality of Karoo magmatism in western Dronning Maud Land, Antarctica. Journal of Volcanology and Geothermal Research 198 (1–2), 1-18.

ACCEPTED MANUSCRIPT

MacDougall, J.D., 1988. Continental Flood Basalts. Kluwer Academic Publishers, Dordrecht, The Netherlands, 341 pp.

Marschall, H.R., Hawkesworth, C.J., Storey, C.D., Dhuime, B., Leat, P.T., Meyer, H.-P., Tamm-Buckle, S., 2010. The Annandagstoppane Granite, East Antarctica: Evidence for Archaean Intracrustal recycling in the Kaapvaal-Grunehogna Craton from zircon O and Hf isotopes. Journal of Petrology 51 (11), 2277-2301.

Maurel, C., Maurel, P., 1982. Étude expérimentale de l'équilibre Fe2+-Fe3+dans les spineless chromiferes et les liquides silicates basiques coexistants, à 1 atm. Comptes Rendus de l'Académie des Sciences (Série 2) 295, 209-212.

Morelli, A., Danesi, S., 2004.Seismological imaging of the Antarctic continental lithosphere: a review. Global and Planetary Change 42 (1-4), 155-165.

Neumann, E-R., Svensen, H., Galerne, C.Y., Planke, S., 2011. Multistage Evolution of Dolerites in the Karoo Large Igneous Province, Central South Africa. Journal of Petrology 52 (5), 959-984.

O'Brien, H.E., Irving, A.J., McCallum, I.S., 1988. Complex zoning and resorption of phenocrysts in mixed potassic mafic magmas of the Highwood Mountains, Montana. American Mineralogist 73, 1007-1024.

O'Hara, M.J., 1968. The bearing of phase equilibria studies in synthetic and natural systems on the origin and evolution of basic and ultrabasic rocks. Earth-Science Reviews 4 (2), 69-133.

Peate, D.W., Baker, J.A., Blichert-Toft, J., Hilton, D.R., Storey, M., Kent, A.J.R., Brooks, C.K., Hansen, H., Pedersen, A.K., Duncan, R.A., 2003. The Prinsen af Wales Bjerge Formation lavas, East Greenland: the transition from tholeiitic to alkalic magmatism during Palaeogene continental break-up. Journal of Petrology 44 (2), 279-304.

ACCEPTED MANUSCRIPT

Prytulak, J., Elliott, T., 2007. TiO2 enrichment in ocean island basalts. Earth and Planetary Science Letters 263 (3-4), 388-403.

Putirka, K.D., 2005. Mantle potential temperatures at Hawaii, Iceland, and the mid-ocean ridge system, as inferred from olivine phenocrysts; evidence for thermally driven mantle plumes. Geochemistry, Geophysics, Geosystems 6 (5), doi:10.1029/2005GC000915.

Putirka, K.D., 2008. Thermometers and barometers for volcanic systems. In: Putirka, K.D. and Tepley, F.J.,III, (Eds.), Minerals, Inclusions and Volcanic Processes. Reviews in Mineralogy and Geochemistry 69, Mineralogical Society of America, pp. 61-120.

Qin, L., Humayun, M., 2008. The Fe/Mn ratio in MORB and OIB determined by ICP-MS. Geochimica et Cosmochimica Acta 72 (6), 1660-1677.

Richards, M.A., Duncan, R.A., Courtillot, V.E., 1989. Flood basalts and hot-spot tracks: plume heads and tails. Science 246, 103-107.

Riley, T.R., Leat, P.T., Curtis, M.L., Millar, I.L., Duncan, R.A., Fazel, A., 2005. Early-Middle Jurassic dolerite dykes from Western Dronning Maud Land (Antarctica): Identifying mantle sources in the Karoo Large Igneous Province. Journal of Petrology 46 (7), 1489-1524.

Salters, V.J.M., Stracke, A., 2004. Composition of the depleted mantle. Geochemistry, Geophysics, Geosystems 5 (5), doi:10.1029/2003GC000597.

Sano, T., Fujii, T., Deshmukh, S.S., Fukuoka, T., Aramaki, S., 2001. Differentiation processes of Deccan Trap basalts: contribution from geochemistry and experimental petrology. Journal of Petrology 42 (12), 2175-2195.

ACCEPTED MANUSCRIPT

Saunders, A.D., 2005. Large igneous provinces: origin and environmental consequences. Elements 1, 259-263.

Simkin, T., Smith, J.V., 1970. Minor-element distribution in olivine. Journal of Geology 78 (3), 304-325.

Sobolev, A.V., Hofmann, A.W., Sobolev, S.V., Nikogosian, I.K., 2005. An olivine-free mantle source of Hawaiian shield basalts. Nature 434, 590-597.

Sobolev, A.V., Hofmann, A.W., Kuzmin, D.V., Yaxley, G.M., Arndt, N.T., Chung, S., Danyushevsky, L.V., Elliott, T., Frey, F.A., Garcia, M.O., Gurenko, A.A., Kamenetsky, V.S., Kerr, A.C., Krivolutskaya, N.A., Matvienkov, V.V., Nikogosian, I.K., Rocholl, A., Sigurdsson, I.A., Sushchevskaya, N.M., Teklay, M., 2007. The amount of recycled crust in sources of mantle-derived melts. Science 316, 412-417.

Storey, M., Mahoney, J.J., Saunders, A.D., 1997. Cretaceous basalts in Madagascar and the transition between plume and continental lithosphere mantle sources. In: Mahoney, J.J. and Coffin, M.F., (Eds.), Large Igneous Provinces: Continental, Oceanic, and Planetary Flood Volcanism. American Geophysical Union, Geophysical Monograph 100, pp. 95-122.

Streck, M.J., 2008. Mineral textures and zoning as evidence for open system processes. In: Putirka, K.D. and Tepley, F.J.,III, (Eds.), Minerals, Inclusions and Volcanic Processes. Reviews in Mineralogy and Geochemistry 69, Mineralogical Society of America, pp. 595-622.

Sun, S.S., McDonough, W.F., 1989. Chemical and isotopic systematics of oceanic basalts: implications formantle composition and processes. In: Saunders, A.D., Norry,M.J. (Eds.), Magmatism in the Ocean Basins. Geological Society Special Publications 42, 313-345.

Sweeney, R.J., Falloon, T.J., Green, D.H., Tatsumi, Y., 1991. The mantle origins of Karoo picrites. Earth and Planetary Science Letters 107 (2), 256-271.

ACCEPTED MANUSCRIPT

Sweeney, R.J., Duncan, A.R., Erlank, A.J., 1994. Geochemistry and petrogenesis of central Lebombo basalts of the Karoo igneous province. Journal of Petrology 35 (1), 95-125.

Thompson, R.N., Gibson, S.A., 2000. Transient high temperatures in mantle plume heads inferred from magnesian olivines in Phanerozoic picrites. Nature 407, 502-506.

Tommasini, S., Manetti, P., Innocenti, F., Abebe, T., Sintoni, M.F., Conicelli, S., 2005. The Ethiopian subcontinental mantle domains: geochemical evidence from Cenozoic mafic lavas. Mineralogy and Petrology 84 (3-4), 259-281.

Tuff, J., Takahashi, E., Gibson, S.A., 2005. Experimental constraints on the role of garnet pyroxenite in the genesis of high-Fe mantle plume derived melts. Journal of Petrology 46 (10), 2023-2058.

Walter, M.J., 1998. Melting of garnet peridotite and the origin of komatiite and depleted lithosphere. Journal of Petrology 39 (1), 29-60.

Watkeys, M.K., 2002. Development of the Lebombo rifted volcanic margin of Southeast Africa. In: Menzies, M.A., Klemperer, S.L., Ebinger, C.J. and Baker, J., (Eds.), Volcanic Rifted Margins. Geological Society of America, Special Publication 362, pp. 27-46.

Wolmarans, L.C., Kent, K.E., 1982. Geological investigations in western Dronning Maud Land, Antarctica - a synthesis. South African Journal of Antarctic Research (Supplements 2), 93 pages.

Wooden, J.L., Czamanske, G.K., Fedorenko, V.A., Arndt, N.T., Chauvel, C., Bouse, R.M., King, B-S.W., Knight, R.J., Siems, D.F., 1993. Isotopic and trace-element constraints on mantle and crustal contributions to Siberian continental flood basalts, Noril'sk area, Siberia. Geochimica Cosmochimica Acta 57 (15), 3677-3704.

Workman, R.K., Hart, S.R., 2005. Major and trace element composition of the depleted MORB mantle (DMM). Earth and Planetary Science Letters 231 (1-2), 53-72.

ACCEPTED MANUSCRIPT

Figure captions

Fig. 1. Outcrop map of western Dronning Maud Land from Vestfjella to H. U. Svedrupfjella with distribution of Karoo flood basalts and Ahlmannryggen Group 3 and Group 4 dikes (one Group 4 dike is also known from Kirwanveggen). Lithospheric boundary between Grunehogna craton and Maud belt is after Corner (1994). Distribution of Karoo flood basalts and related intrusive rocks (outside the flood basalt areas) in reconstructed Gondwana supercontinent (cf. Heinonen et al., 2010) is shown in the inset.

Fig. 2. Geochemical characteristics of the Ahlmannryggen Group 3 and 4 dikes shown in TiO_2 vs. MgO diagram (a), FeO_{tot} vs. MgO diagram (b), primitive mantle –normalized (Sun and McDonough, 1989) trace element spider diagram (c), and initial ε_{Nd} vs. $^{87}Sr/^{86}Sr$ (at 180 Ma) diagram (d). Data for Antarctic Karoo CFBs (a, b, d; Harris et al., 1990; Luttinen et al., 1998, 2010; Luttinen and Furnes, 2000), Vestfjella depleted (D-FP) and enriched (E-FP) ferropicrite suites (a–d, samples AL/B9-03 and JSH/B006 in b; Heinonen and Luttinen, 2008; Heinonen et al., 2010), average N-MORB and OIB (c; Sun and McDonough, 1989), SWIR MORB (d; compiled from the Petrological Database of the Ocean Floor, http://www.petdb.org), and depleted mantle (DM in d; Workman and Hart, 2005) also presented. Melts with TiO_2 > 2 wt. % are not likely to derive solely from depleted or pyrolitic mantle peridotite (Prytulak and Elliott, 2007; Walter, 1998).

Fig. 3. Some petrographic and mineral chemical features of the Ahlmannryggen Group 3 and 4 dikes: (a) Glomeroporphyritic olivine and an orthopyroxene phenocryst in micro- to cryptocrystalline groundmass (Sample Z1825.3; plane-polarized light); (b) Pyroxene phenocryst that mostly consists of clinopyroxene (light grey), but contains irregular inclusions of orthopyroxene (dark grey) and altered olivine (grey, high relief). Groundmass consists of clinopyroxene (light grey), plagioclase (very dark grey), and Fe-Ti oxides (white). Olivine phenocryst is partially visible in the upper left corner. (Sample Z1817.2; BSE image); (c) Oscillatory-zoned orthopyroxene phenocrysts with clinopyroxene rims; (d) Compositional profile from c to c' (Sample Z1812.3; BSE image); (e) Weakly-zoned orthopyroxene phenocryst with thin clinopyroxene rim; (f) Compositional profile from e to e' (Sample Z1816.3; BSE image); (g) Progressively-zoned olivine phenocryst in a groundmass consisting of microcrystalline pyroxene (light grey) and Fe-Ti oxides (white)

ACCEPTED MANUSCRIPT

and glass (dark grey); (h) Compositional profile from g to g' (Sample Z1826.1; BSE image). Limit of detection (LOD) shown for Cr_2O_3 and NiO (cf. Electronic Appendix A).

Fig. 4. Olivine Fo vs. whole-rock Mg# diagram and sample-specific olivine histograms for the Ahlmannryggen Group 3 and 4 dikes (only core compositions are taken into account). Large squares indicate average Fo content; averages of two distinct populations are shown in the case of Z1826.1 and only the average of the low-Mg population is shown in the case of Z1816.3. Group 3 samples Z1803.3, Z1812.1, and Z1812.3 do not contain fresh olivine and are thus not plotted. $K_d(Fe^{2+}\text{-}Mg)^{ol\text{-}liq}$ values for the equilibration curves (0.29, 0.32, 0.35) are the ones recommended by Putirka (2005) for a pressure range of 0–8 GPa.

Fig. 5. Olivine NiO vs. Fo diagram of the Ahlmannryggen Group 3 and 4 dikes. Group 3 has been divided into three subgroups on the basis of olivine NiO contents. Reference data for olivines found in Vestfjella depleted (D-FP) and enriched (E-FP) ferropicrite suites (Heinonen and Luttinen 2010; Heinonen et al., 2010), MORB (Sobolev et al., 2007; see references therein), and Mauna Kea (Sobolev et al., 2007; see references therein) also shown. Limit of detection shown (LOD) for NiO (cf. Electronic Appendix A).

Fig. 6. Orthopyroxene Mg# vs. whole-rock Mg# diagram for the Ahlmannryggen Group 3 and 4 dikes (crystal rim compositions are not taken into account). Large squares indicate average orthopyroxene Mg# content. Group 3 samples Z1803.1 and Z1803.5 and Group 4 sample Z1838.1 do not contain orthopyroxene and are thus not plotted. $K_d(Fe^{2+}\text{-}Mg)^{opx\text{-}liq}$ values for the equilibration curves (0.29 ± 0.06) are the ones recommended by Putirka (2008) on the basis of experimental data.

Fig. 7. Pyroxenes of the Ahlmannryggen Group 3 and 4 dikes and Mwenezi picrites (Cox and Jamieson, 1974) in the Enstatite-Ferrosilite-Wollastonite ternary diagram.

Fig. 8 Cr-spinel chemistry of the Ahlmannryggen Group 3 and 4 dikes and Vestfjella depleted ferropicrite suite (Heinonen and Luttinen, 2010) shown in the TiO_2 vs. Al_2O_3 diagram. Spinel discrimination fields (LIP = large igneous provinces; OIB = oceanic island basalts; MORB = mid-ocean ridge basalts; ARC = island arcs; Peridotites = mantle peridotites) are after Kamenetsky et al. (2001).

ACCEPTED MANUSCRIPT

Fig. 9 PELE-modeled liquidus curves of olivine (ol), orthopyroxene (opx), clinopyroxene (cpx), and plagioclase (plg) in hypothetical parental magmas corresponding to samples Z1803.1, Z1825.3, and Z1838.1 shown in T vs. P diagrams. Although sample Z1813.1 was also modeled, it is not shown as it crystallizes orthopyroxene before clinopyroxene only in pressures of > 6 kbar (cf. section 5.2.). Grey area indicates the pressure space that is compatible with the petrographic evidence. Unlikely models marked with parentheses.

Fig. 10. Whole-rock CaO vs. MgO diagram of the Ahlmannryggen Group 3 and Group 4 dikes and hypothetical primary melts calculated for them (Table 3). High-Ni^{ol}, medium-Ni^{ol}, and low-Ni^{ol} Group 3 samples (cf. Fig. 5), melt-representative samples Z1803.1 (Group 3) and Z1825.3 (Group 4), and cumulate sample Z1816.3 (Group 3) are indicated; sample Z1816.3 has been accumulation-corrected for this diagram (cf. section 7.2.); accumulation corrections for other samples would pose negligible changes in terms of PX#. Vestfjella depleted (D-FP) and enriched (E-FP) ferropicrite suite (samples that exhibit olivine compositional data; Heinonen and Luttinen, 2010, Heinonen et al., 2010) and fractionation vectors for olivine, orthopyroxene, clinopyroxene, and plagioclase are also indicated. Stippled field indicates olivine-orthopyroxene addition vectors of the hypothetical primary melt modeling (cf. section 7.1. and Table 3). Peridotite and pyroxenite partial melt fields after Herzberg and Asimow (2008); "forbidden field" indicates pyroxenite partial melt compositions that are excessively Mg-rich and have not been produced experimentally.

Fig. 11. Olivine NiO vs. PX# (a) and Zn/Fe vs. PX# (b) diagrams of the Ahlmannryggen Group 3 and Group 4 dikes. High-Ni^{ol}, medium-Ni^{ol}, and low-Ni^{ol} Group 3 samples (cf. Fig. 5), melt-representative samples Z1803.1 (Group 3) and Z1825.3 (Group 4), and cumulate sample Z1816.3 (Group 3) are indicated; sample Z1816.3 has been accumulation-corrected (cf. Fig. 10) ($K_d(Zn)^{ol\text{-}liq} = K_d(Zn)^{opx\text{-}liq} = 1$; Le Roux et al., 2011). Vestfjella depleted (D-FP) and enriched (E-FP) ferropicrite suite (samples that exhibit olivine compositional data; Heinonen and Luttinen, 2010, Heinonen et al., 2010) and average MORB (olivine NiO compiled from the Petrological Database of the Ocean Floor: http://www.petdb.org; PX# after Salters and Stracke, 2004; Zn/Fe after Le Roux et al., 2010) and Mauna Kea basalt/picrite (compiled from GEOROC database: http://georoc.mpchmainz.gwdg.de/georoc/) also shown. The differences in

ACCEPTED MANUSCRIPT

olivine NiO between different localities may partly stem from the differences in the pressure of partial melting below continental and oceanic lithosphere (cf. D-FP and MORB; Li and Ripley, 2010); the relative effects of these factors (source composition and pressure of melting) are difficult to constrain.

ACCEPTED MANUSCRIPT

ACCEPTED MANUSCRIPT

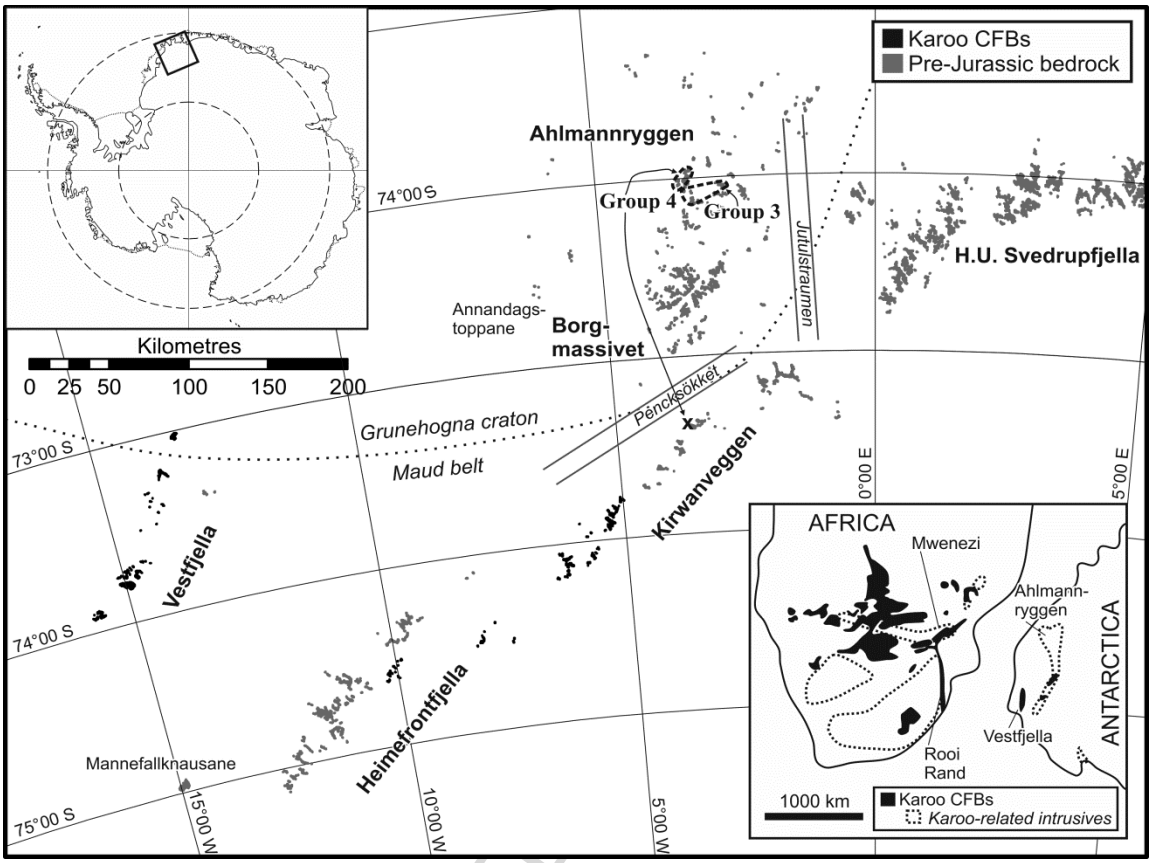

Figure 1

ACCEPTED

ACCEPTED MANUSCRIPT

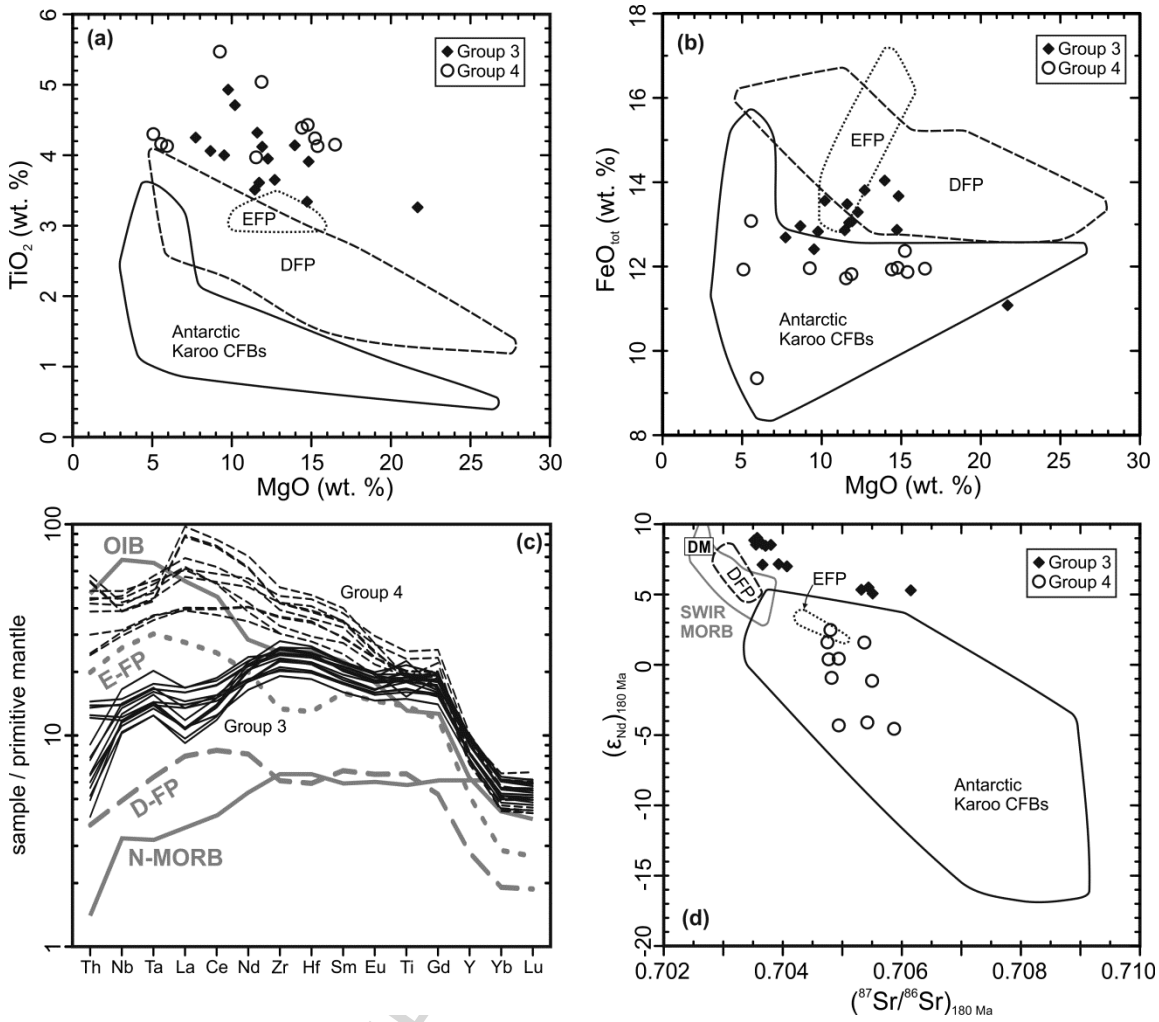

Figure 2

ACCEPTED

ACCEPTED MANUSCRIPT

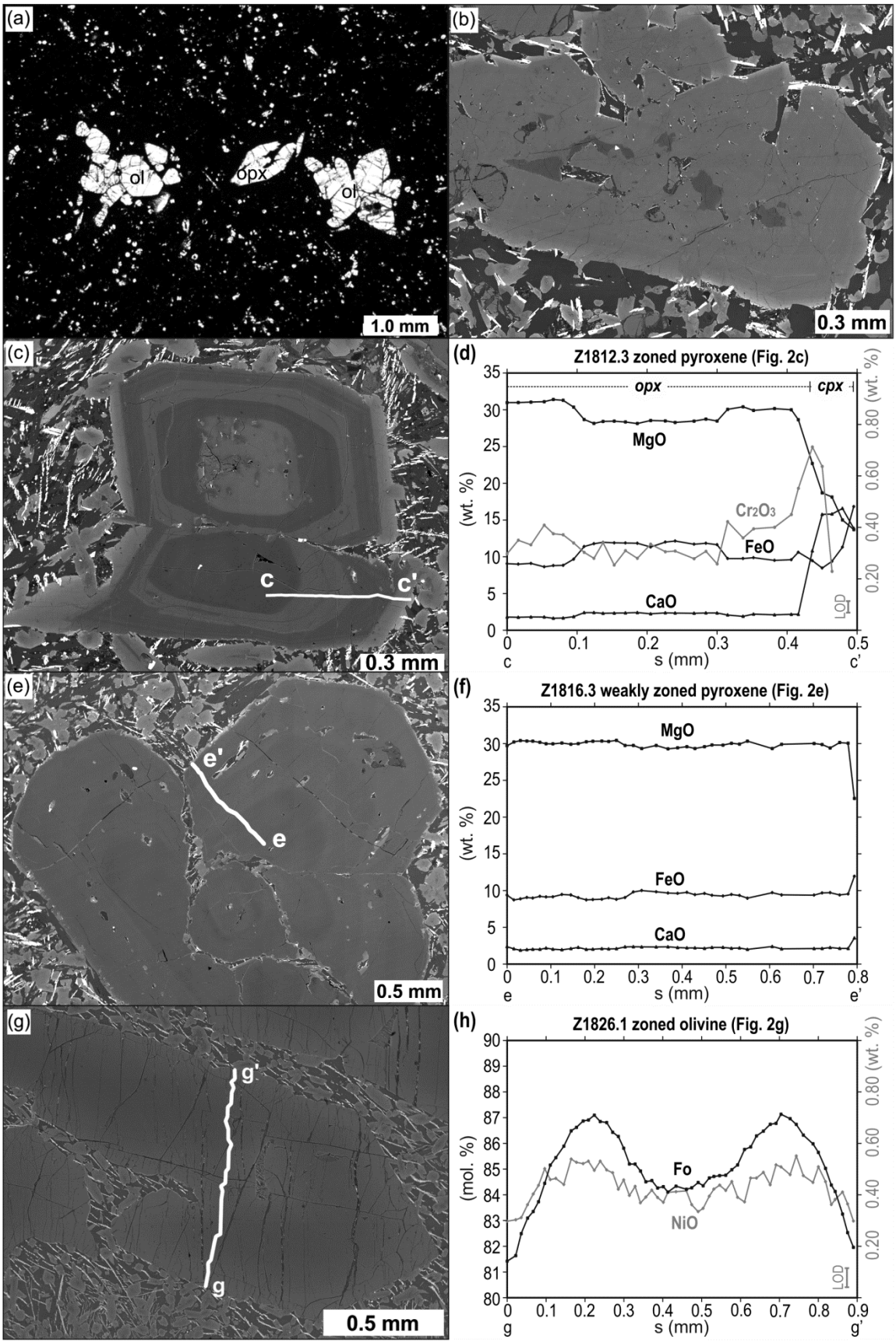

Figure 3

ACCEPTED MANUSCRIPT

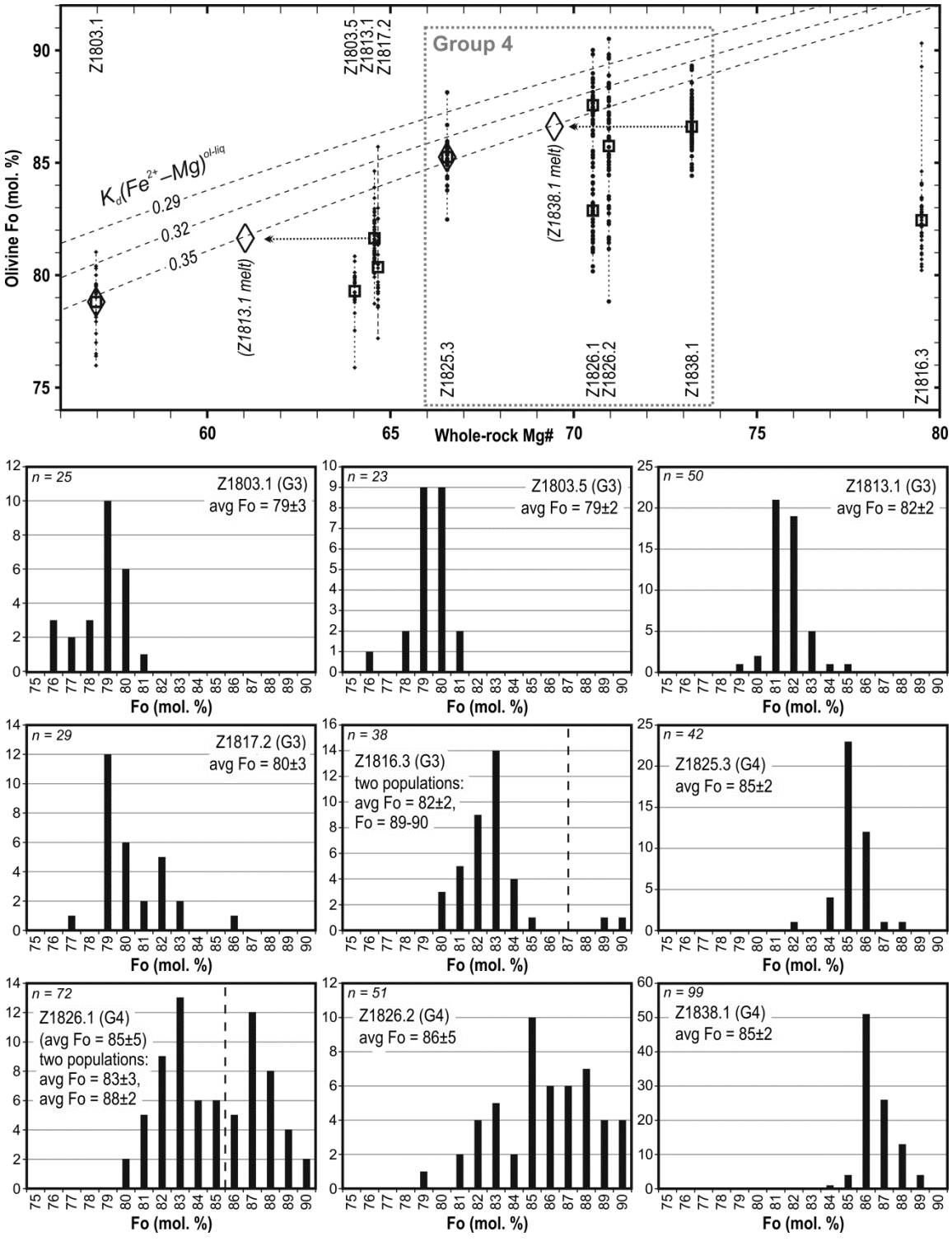

Figure 4

ACCEPTED MANUSCRIPT

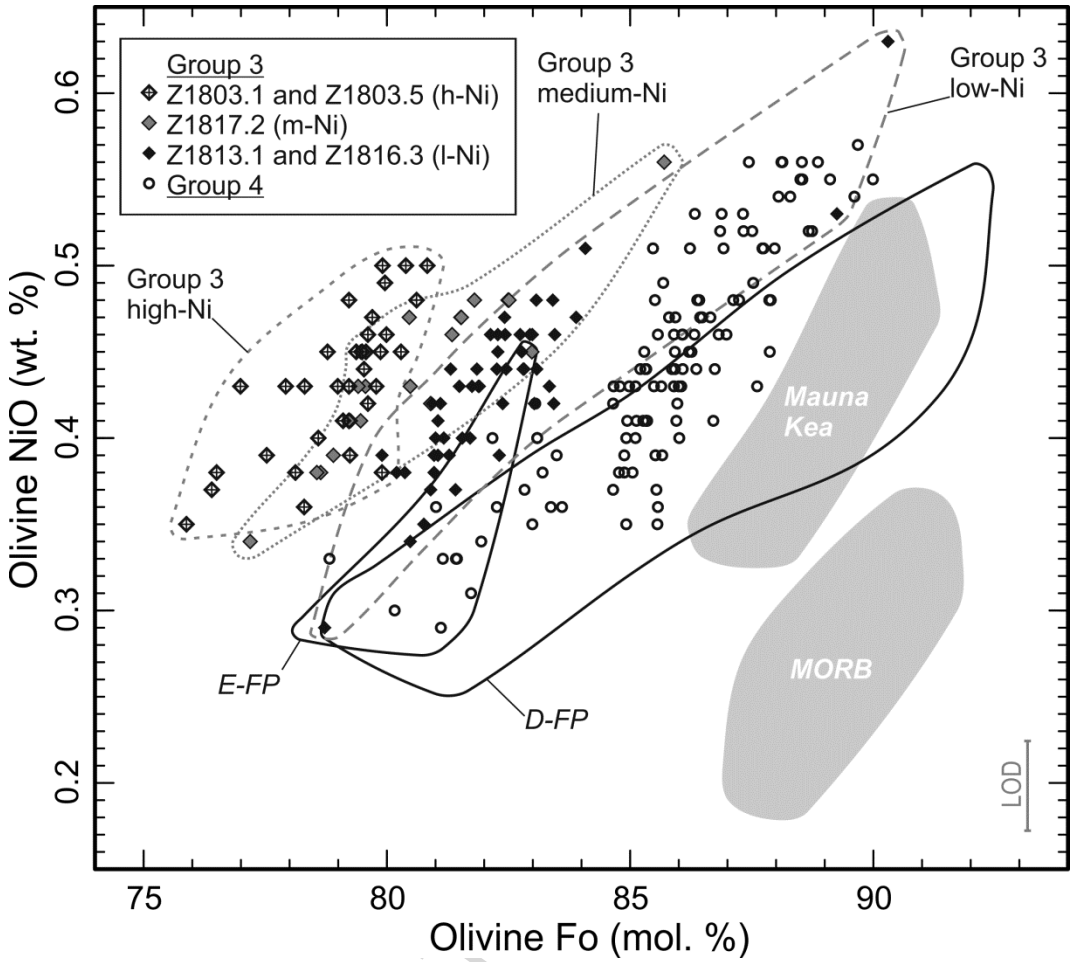

Figure 5

ACCEP

ACCEPTED MANUSCRIPT

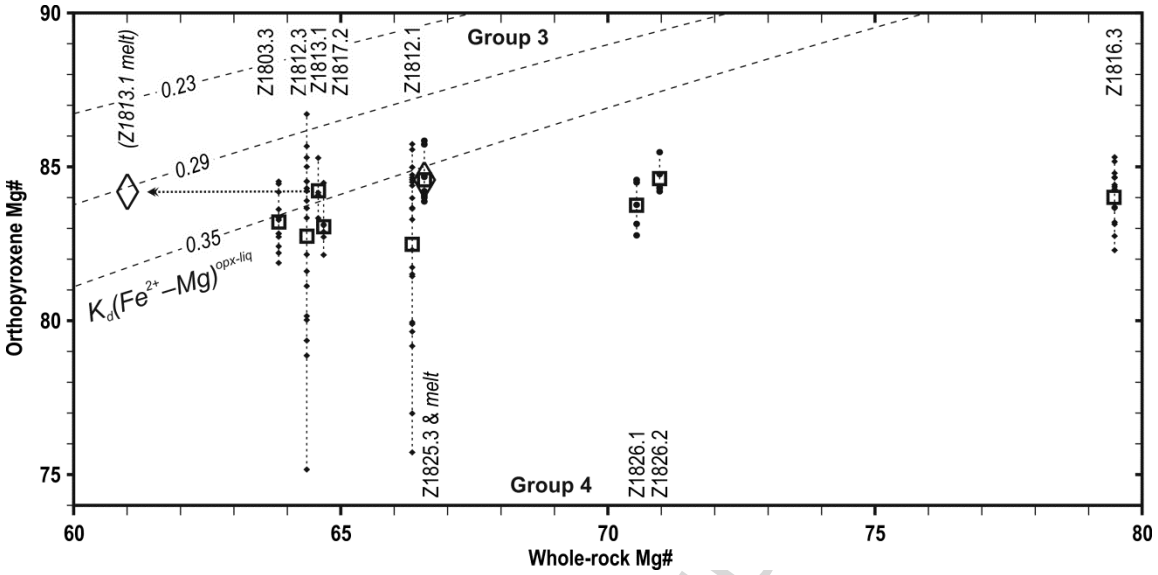

Figure 6

ACCEPTED MANUSCRIPT

ACCEPTED MANUSCRIPT

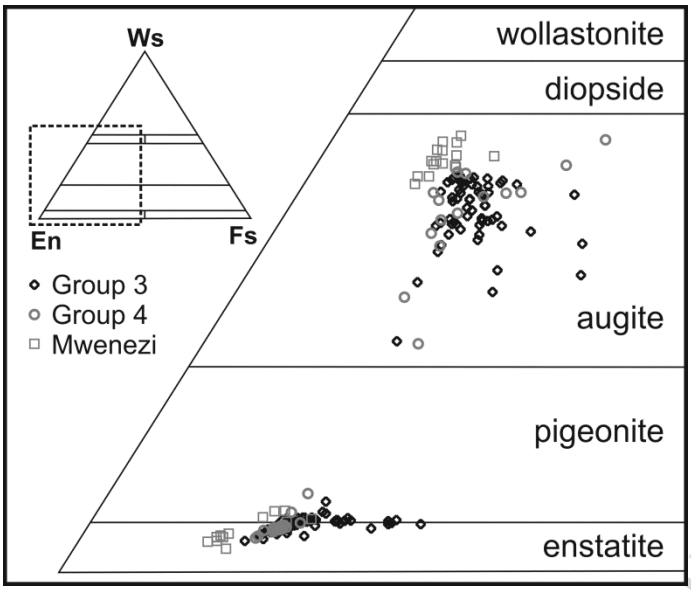

Figure 7

ACCEPTED MANUSCRIPT

ACCEPTED MANUSCRIPT

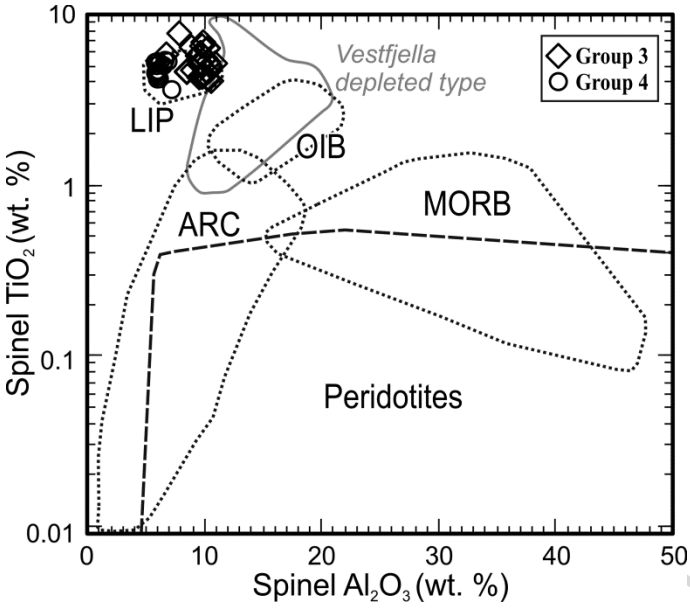

Figure 8

ACCEPTED MANUSCRIPT

ACCEPTED MANUSCRIPT

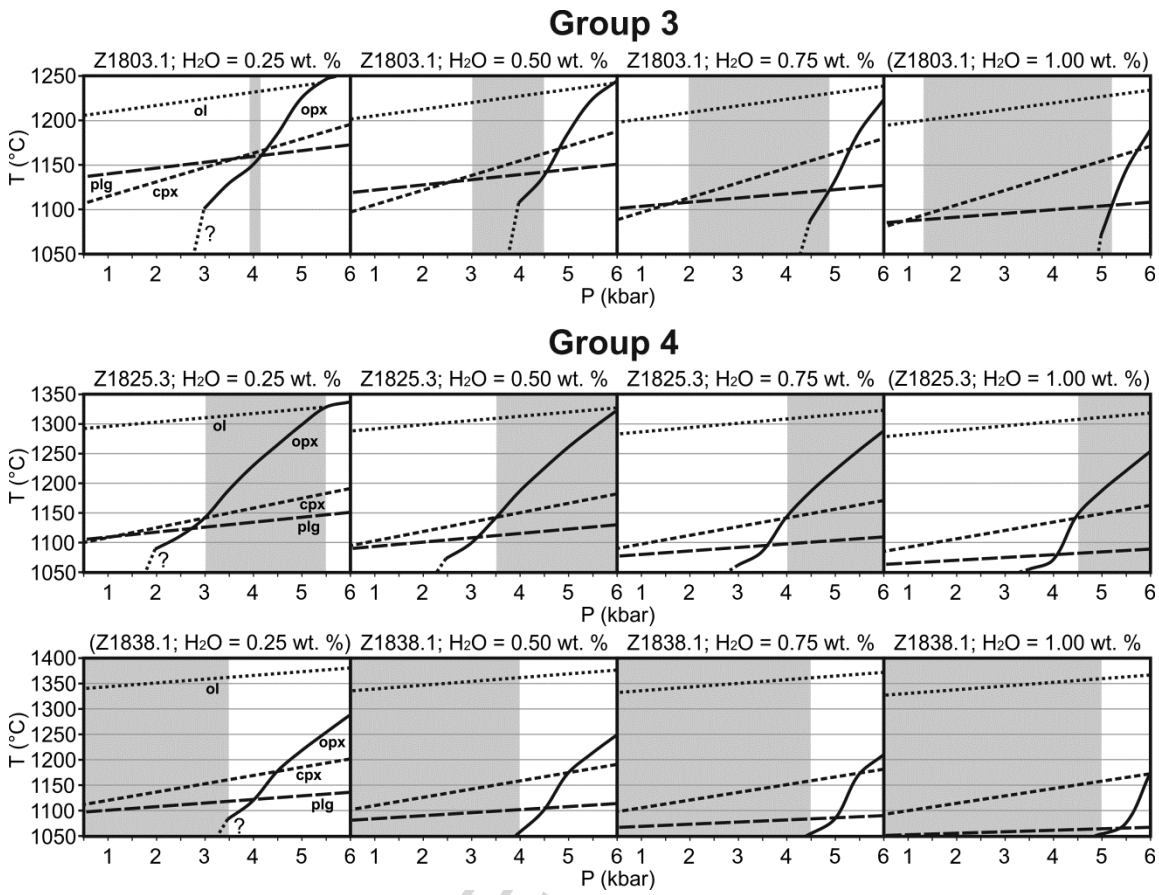

Figure 9

ACCEPTED

ACCEPTED MANUSCRIPT

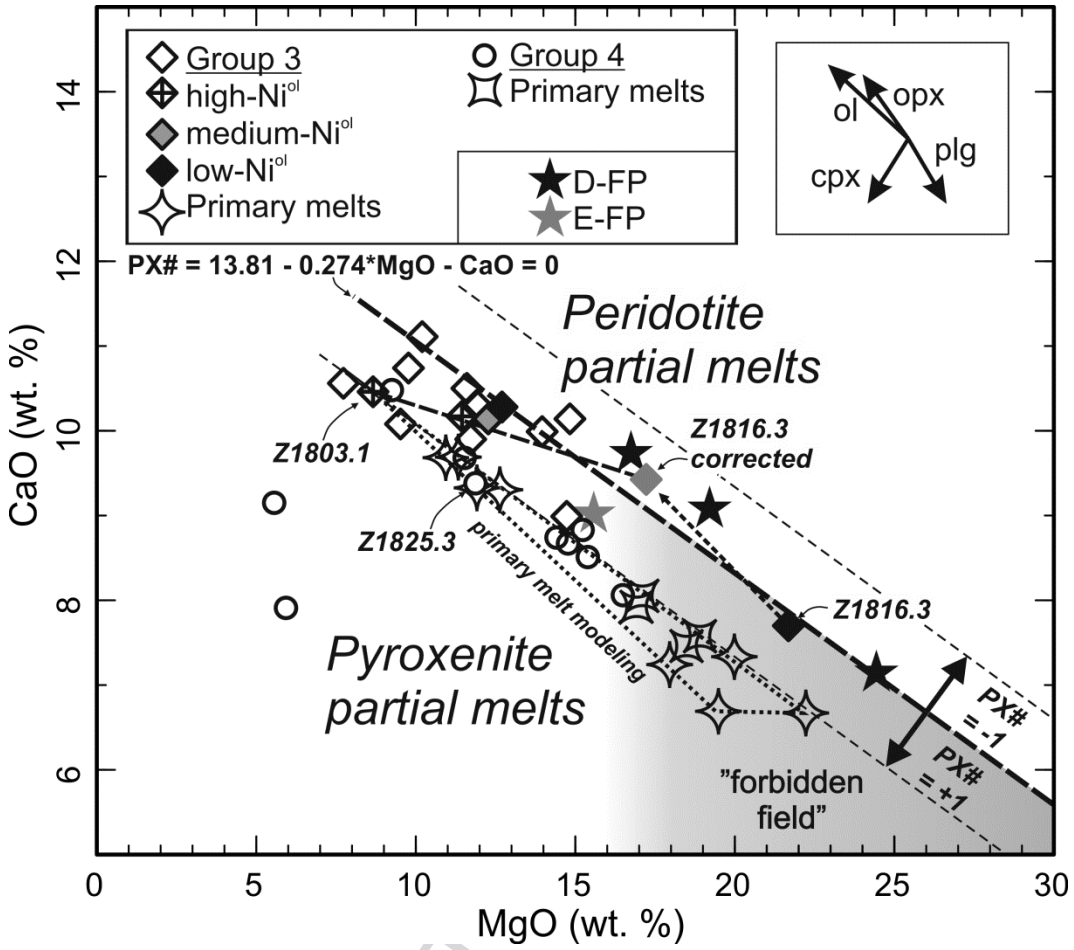

Figure 10

ACCEPTED

ACCEPTED MANUSCRIPT

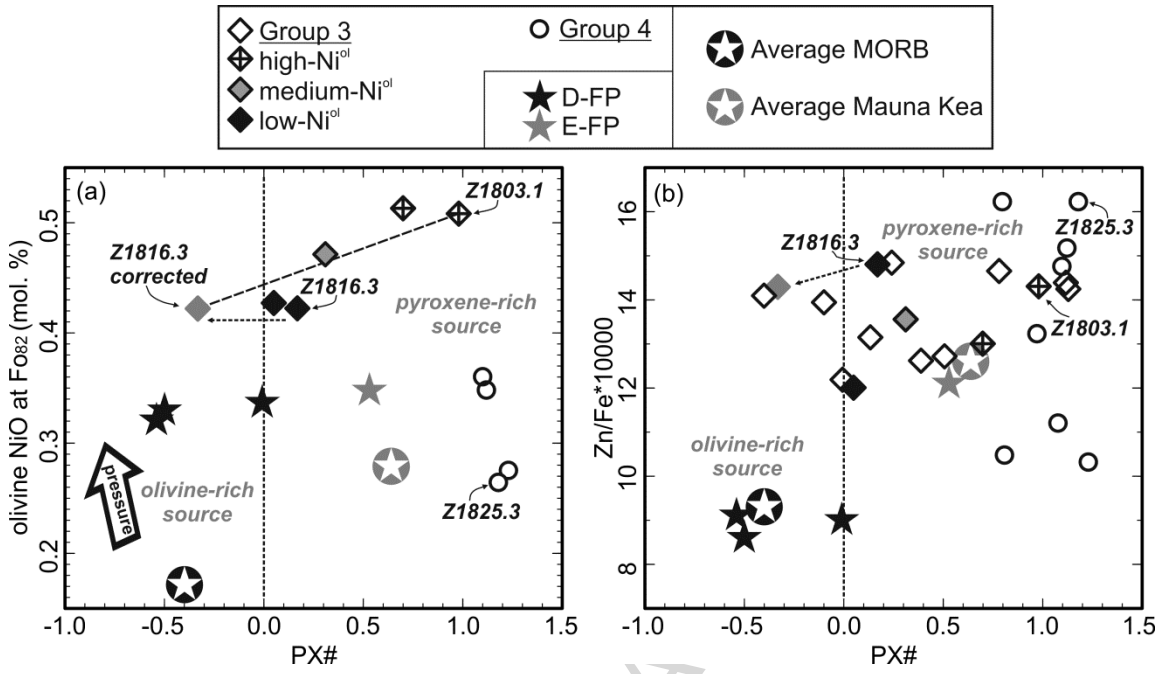

Figure 11

ACCEPTED MA

ACCEPTED MANUSCRIPT

Table 1 Whole-rock major and minor element data for the Ahlmannryggen Group 3 and Group 4 picrite dikes selected for mineral chemical analysis (Riley et al., 2005)

Sample	Z1803.1	Z1803.3	Z1803.5	Z1812.1	Z1812.3	Z1813.1	Z1816.3	Z1817.2	Z1825.3	Z1826.1	Z1826.2	Z1838.1
Group	III	III	III	III	III	III	III	III	IV	IV	IV	IV
Major and minor elements (wt. %, normalized to 100% volatile free)												
SiO_2	49.15	49.68	48.85	47.39	49.17	47.11	45.94	47.60	49.45	49.33	49.28	48.26
TiO_2	4.06	3.51	3.61	4.14	4.12	3.65	3.26	3.95	5.04	4.39	4.43	4.15
Al_2O_3	12.02	9.95	10.54	8.46	9.49	9.99	8.17	10.45	9.63	8.81	8.65	7.82
FeO_{tot}	12.96	12.86	13.04	14.04	13.07	13.81	11.08	13.29	11.82	11.93	11.97	11.95
MnO	0.17	0.17	0.17	0.20	0.17	0.18	0.18	0.17	0.15	0.15	0.15	0.16
MgO	8.66	11.45	11.72	13.96	11.91	12.70	21.68	12.27	11.87	14.41	14.77	16.49
CaO	10.46	10.17	9.90	9.99	10.30	10.28	7.70	10.14	9.38	8.74	8.67	8.06
Na_2O	1.84	1.66	1.68	1.36	1.34	1.72	1.25	1.61	1.73	1.47	1.33	1.90
K_2O	0.44	0.35	0.28	0.21	0.18	0.33	0.55	0.28	0.57	0.43	0.42	0.83
P_2O_5	0.24	0.22	0.22	0.25	0.24	0.23	0.19	0.25	0.36	0.34	0.34	0.37
Total**	100.50	100.04	100.40	99.50	100.50	99.40	99.50	100.00	100.40	100.60	100.25	99.60
LOI	0.69	1.07	1.05	1.69	1.05	1.93	1.28	0.77	1.85	2.05	1.91	2.28
Mg#*	57	64	64	66	64	65	79	65	67	71	71	73

* Mg# = Mg-number [atomic $Mg/(Mg+Fe^{2+})*100$; $Fe^{2+}/Fe_{tot}=0.9$]. ** before normalization and including loss-on-ignition (LOI)

ACCEPTED MANUSCRIPT

ACCEPTED MANUSCRIPT

Table 2 Petrographic characteristics of the Ahlmannryggen Group 3 and Group 4 dikes

Sample	phenocrysts	groundmass	olivine pcs	opx pcs	cpx pcs
Z1803.1 (III)	8%ol, 13%cpx	79%*	≤1 mm	-	≤0.5mm
Z1803.3 (III)	(2%ol), 6%opx	(10%ol), 40%cpx, 34%pl, 10%opq	≤1.5 mm	≤3 mm, thick cpx rims	-
Z1803.5 (III)	3%ol, 12%cpx, 1%pl	84%*	≤0.5 mm	-	≤0.5mm
Z1812.1 (III)	(6%ol), 18%opx	43%opx+cpx, 19%pl, 14%opq	≤2 mm	≤3 mm, z, thin cpx rims	-
Z1812.3 (III)	(2%ol), 7%opx	47%opx+cpx, 18%pl, 26%opq	≤1.5 mm	≤3.5 mm, z, thin cpx rims	-
Z1813.1 (III)	10%ol, 4%opx	37%cpx, 35%pl, 14%opq	≤2 mm	≤3 mm, wz, thin cpx rims	-
Z1816.3 (III)	12%ol, 15%opx	32%cpx, 29%pl, 12%opq	≤2 mm	≤4 mm, wz, thin cpx rims	-
Z1817.2 (III)	8%ol, 12%opx+cpx	30%cpx, 28%pl, 22%opq	≤1.5 mm	≤2.5 mm, thick cpx rims	≤1.5mm
Z1825.3 (IV)	4%ol, 3%opx	93%*	≤2 mm	≤2.5 mm, thin cpx rims	-
Z1826.1 (IV)	9%ol, 2%opx	89%*	≤2 mm, 2 types	≤1 mm, thin cpx rims	-
Z1826.2 (IV)	8%ol, 4%opx	88%*	≤2 mm, 2 types	≤1 mm, thin cpx rims	-
Z1838.1 (IV)	28%ol	72%*	≤1 mm	-	-

pcs = phenocrysts, ol = olivine (parentheses indicates olivine pseudomorphs), opx = orthopyroxene (mantled by clinopyroxene), cpx = clinopyroxene, pl = plagioclase, opq = Fe-Ti oxides; z = zoned, wz = weakly zoned; * mineral grains too fine-grained to identify in an optical microscope

ACCEPTED MANUSCRIPT

ACCEPTED MANUSCRIPT

Table 3 Primary melt compositions calculated for Ahlmannryggen Group 3 and Group 4 dikes.

	Starting compositions (parental melts)				Calculated primary melts											
Sample	Z1803.1	Z1825.3	Z1813.1*	Z1838.1*	Z1803.1	Z1803.1	Z1803.1	Z1803.1	Z1803.1	Z1803.1	Z1803.1	Z1803.1	Z1825.3	Z1825.3	Z1825.3	Z1825.3
Group	III	IV	III	IV	III	III	III	III	III	III	III	III	IV	IV	IV	IV
olivine-liq K_d	-	-	-	-	K_d=0.32	K_d=0.35	K_d=0.32	K_d=0.35	K_d=0.32	K_d=0.35	K_d=0.32	K_d=0.35	K_d=0.32	K_d=0.35	K_d=0.32	K_d=0.35
equilibrium olivine	-	-	-	-	Fo_{90}	Fo_{90}	Fo_{90}	Fo_{90}	Fo_{84}	Fo_{84}	Fo_{84}	Fo_{84}	Fo_{90}	Fo_{90}	Fo_{90}	Fo_{90}
fractionating assemblage	-	-	-	-	31% ol	38% ol	9% ol 26% opx	10% ol 31% opx	8% ol	12% ol	2% ol 6% opx	3% ol 9% opx	15% ol	20% ol	11% ol 7% opx	14% ol 9% opx
SiO_2 (wt. %)	49.15	49.45	47.33	48.99	46.50	45.83	50.28	50.46	48.43	48.06	49.41	49.52	48.22	47.70	49.07	48.89
TiO_2	4.06	5.04	3.91	4.56	2.81	2.54	2.72	2.49	3.75	3.59	3.73	3.59	4.29	4.03	4.20	3.93
Al_2O_3	12.02	9.63	10.70	8.57	8.31	7.52	8.14	7.47	11.10	10.64	11.08	10.65	8.21	7.71	8.00	7.48
FeO(tot)	12.96	11.82	13.71	11.87	13.23	13.54	11.92	11.80	13.29	13.45	12.76	12.70	11.77	11.86	11.61	11.62
MnO	0.17	0.15	0.18	0.15	0.15	0.14	0.17	0.17	0.16	0.16	0.17	0.17	0.15	0.14	0.15	0.14
MgO	8.66	11.87	10.74	13.63	19.96	22.21	17.92	19.46	11.26	12.58	10.87	11.86	17.07	18.87	16.88	18.45
CaO	10.46	9.38	10.98	8.82	7.31	6.64	7.22	6.66	9.68	9.29	9.67	9.31	8.03	7.56	7.90	7.43
Na_2O	1.84	1.73	1.85	2.08	1.27	1.15	1.20	1.09	1.70	1.63	1.68	1.61	1.47	1.38	1.43	1.33
K_2O	0.44	0.57	0.36	0.91	0.30	0.28	0.29	0.26	0.41	0.39	0.40	0.39	0.48	0.45	0.47	0.44
P_2O_5	0.24	0.36	0.25	0.41	0.17	0.15	0.16	0.14	0.22	0.21	0.22	0.21	0.31	0.29	0.30	0.28
Mg#**	57	67	61	69	75	76	75	77	63	65	63	65	74	76	74	76

* only used in PELE modeling; ** Mg# = Mg/(Mg+0.9*Fe)*100

ACCEPTED MANUSCRIPT

ACCEPTED MANUSCRIPT

Highlights

Continental flood basalt –related dikes crystallized from high-Mg magmas

The dikes were emplaced at crustal depths of 10–20 km

Pyroxene-rich components were essential in the mantle sources

Some of the magmas sampled mixed pyroxenite-peridotite sources

ACCEPTED MANUSCRIPT